Swiss J Geosci (2017) 110:39–66
DOI 10.1007/s00015-016-0248-x

Tectonic evolution around the Mont Terri rock laboratory, northwestern Swiss Jura: constraints from kinematic forward modelling

Christophe Nussbaum[1] · Armelle Kloppenburg[2] · Typhaine Caër[3] · Paul Bossart[1]

Received: 10 April 2016 / Accepted: 9 December 2016 / Published online: 28 January 2017

Abstract We propose a geometrically, kinematically, and mechanically viable thin-skinned kinematic forward model for a cross section intersecting the Mont Terri rock laboratory in the frontal-most part of the Jura fold-and-thrust belt, Switzerland. In addition to the available tunnel, borehole, and surface data, initial boundary conditions are crucial constraints for the forward modelling scenarios, especially the inherited topography of the basement and any pre-compressional offset within the Mesozoic sediments. Our kinematic analysis suggests an early-stage formation of the Mont Terri anticline located above ENE-trending, Late Paleozoic extensional faults, followed by back-stepping of the deformation developing the Clos du Doubs and Caquerelle anticlines further south. In this model, the thrust sequence was dictated by the inherited basement faults, which acted as nuclei for the ramps, detached along the basal décollement within the Triassic evaporites. The mechanical viability of both the thrust angles and thrust sequence was demonstrated by applying the limit analysis theory. Despite numerous subsurface geological data, extrapolation of structures to depth remains largely under-constrained. We have tested an alternative model for the same cross section, involving an upper detachment at the top of the Staffelegg Formation that leads to duplication of the sub-Opalinus Clay formations, prior to detachment and thrusting on the Triassic evaporites. This model is geometrically and kinematically viable, but raises mechanical questions. A total displacement of 2.9 and 14.2 km are inferred for the classical and the alternative scenarios, respectively. In the latter, forward modelling implies that material was transported 10.8 km along the upper detachment. It is not yet clear where this shortening might have been accommodated. Despite the differences in structural style, both models show that pre-existing basement structures might have interfered in time and space. Both styles may have played a role, with lateral variation dictated by basement inherited structures.

Keywords Jura mountains · Structural geology · Multiple detachments · Forward modelling · Inherited basement faults · Mechanical analysis

1 Introduction

This study addresses the tectonic evolution of the region around the Mont Terri underground rock laboratory where experiments are dedicated to investigating the hydrogeological, geochemical, and rock mechanical properties of a pristine undisturbed claystone, the Opalinus Clay of Toarcian-Aalenian age (Bossart and Thury 2008; Bossart et al. 2017). The generic Mont Terri underground rock laboratory offers a scientific and technical platform for international collaboration in the field of geological disposal providing a unique opportunity to study the performance of a repository. The Mont Terri rock laboratory is located in the northern part of the Jura fold-and-thrust belt at the southern tip of the Upper Rhine Graben (Nussbaum et al. 2011).

Editorial handling: P. Bossart and A. G. Milnes.

This is paper #2 of the Mont Terri Special Issue of the Swiss Journal of Geosciences (see Bossart et al. 2017, Table 3 and Fig. 7.

✉ Christophe Nussbaum
christophe.nussbaum@swisstopo.ch

[1] Swiss Geological Survey, Federal Office of Topography Swisstopo, Seftigenstrasse 264, 3084 Wabern, Switzerland

[2] 4DGeo/Structural Geology, Daal en Bergselaan 80, 2565 AH The Hague, The Netherlands

[3] Géosciences et Environnement Cergy (GEC), Université de Cergy-Pontoise, rue Descartes, 95031 Cergy-Pontoise Cedex, France

The arcuate Jura mountain range is considered as a type example of a thin-skinned fold-and-thrust belt that propagates into the northern foreland of the Alpine orogeny along a basal décollement horizon formed by the mechanically weak Middle and Upper Triassic stratigraphic units (Buxtorf 1907; Laubscher 1961; Burkhard 1990; Guellec et al. 1990; Jordan 1992; Philippe 1995; Sommaruga and Burkhard 1997; Becker 2000). Thin-skinned deformation along this basal detachment is considered to have started not earlier than the Serravallian (Middle Miocene) and to have ceased in the Early Pliocene (e.g. Laubscher 1992; Becker 2000). Many authors postulate a late transition (post-early Pliocene) to thick-skinned tectonics (e.g. Mosar 1999; Ustaszewski and Schmid 2007; Madritsch et al. 2008) based on field observation and interpretation of seismic reflection data. Already in 1990, Guellec et al. proposed a transition from thin-skinned to thick-skinned deformation involving basement thrusts beneath the Internal Jura at Champfromier (south to Oyonnax) to explain a basement high interpreted on a seismic profile. The Jura has often been considered a foreland fold-and-thrust belt propagating from south to north. Nevertheless, this classical view is a matter of debate and certain authors, such as Cederboom et al. (2011), convincingly showed that the subalpine Molasse has been active after 5 Ma demonstrating "out-of-sequence" thrust chronology. By analogue modelling, Smit et al. (2003) suggested that the order of thrusts depends on many factors such as basal wedge angle, shortening rate, and coupling between basement and cover.

Over the last four decades, foreland fold-and-thrust belts have been modelled as critically tapered wedges (Chapple 1978; Boyer and Elliot 1982). The geometry of a critical wedge is defined by its surface slope and the dip of the basal décollement. Both depend on basal friction and material of the wedge, its density, and shear strength (Chapple 1978; Davis et al. 1983; Dahlen 1990). As a consequence, tectonic evolution and kinematics of thin-skinned fold-and-thrust belts are strongly controlled by the thickness of the sedimentary cover overlying the basal décollement, eventually modified by syn-tectonic erosion or sedimentation as well as aspects influencing the basal friction of the décollement, such as fluid pressure and fracture strength (Sommaruga and Burkhard 1997; Hindle 2008; von Hagke et al. 2014). In addition to these principal controlling mechanisms, localisation and development of contractional structures in thin-skinned foreland fold-and-thrust belts is known to be commonly influenced by pre-existing structures (i.e. Butler et al. 2006; Giambiagi et al. 2003). Deformation events predating thrust-belt initiation affect the geometry of the basal décollement horizon, potentially even offsetting it, and lead to the formation of fractures and faults that can act as pre-existing zones of mechanical weakness during thrust-belt formation (Laubscher 1985, 1987; Homberg et al. 2002; Ustaszeswki and Schmid 2007; Madritsch et al. 2008).

In 2003, Freivogel and Huggenberger proposed an initial interpretation of the deep structures beneath the Mont Terri rock laboratory based on a balanced cross section of the Mont Terri anticline along the Mont Terri motorway tunnel. They interpreted the Mont Terri anticline as a NNW-vergent imbricate fault-bend fold, with a total shortening estimated by area balancing to be approximately 2.1 km. Later, Caër et al. (2015) proposed two alternative 2D kinematic models for the same structure, interpreting it as the result of various combinations of fault-bend folding, fault-propagation folding, and detachment folding. Their interpretation is significantly different, since they considered inherited basement normal faults to play an active role during folding (thick-skinned deformation). They estimated a total shortening of 1.2–1.3 km for the Mont Terri anticline. They validated the mechanical viability of the sections by a mechanical approach using limit analysis theory described below in Sect. 6.1.

Here, we present new insights into the tectonic evolution of the region around the Mont Terri rock laboratory based on a combined analysis of geological maps, available data collected during the excavation of the Mont Terri and Mont Russelin tunnels, drilling of the reconnaissance boreholes, cross section area balancing techniques, and kinematic forward modelling. Whereas the rock laboratory and the tunnels provide a unique access to fresh and continuous outcrops, the underlying structure remains under-constrained. There are few seismic profiles available for the study region but their resolution, especially at the base of Mesozoic sequence, is insufficient for any interpretation of deep structures. Therefore, sequential restoration of cross sections is not possible, and any kinematic modelling must be concept-driven, starting from the available geological constraints. We propose here a kinematic forward model using the available data augmented by limiting constraints at depth. The aim of the kinematic modelling is to understand the dominant structural style, the sequence of thrusts and the kinematic relationships of the structural elements that are exposed and have been mapped around the Mont Terri rock laboratory.

2 Regional geological setting

2.1 Inherited Palaeozoic and Paleogene basement structures

The study region near the Mont Terri rock laboratory is characterized by a complex tectonic setting resulting from the junction of the northernmost part of the Folded Jura

with the southern end of the Upper Rhine Graben (URG) (top right inset in Fig. 1). At least two major inherited basement structures have affected the thin-skinned deformation of the Jura fold-and-thrust belt emplaced during Late Miocene-Early Pliocene times. The first inherited basement structure is related to Late Palaeozoic ENE-to NE-oriented basement faults from the Variscan orogeny and subsequent (Late Carboniferous to Permian) post-orogenic extension (Laubscher 1985; Ziegler 1992; Schumacher 2002). The second inheritance mainly re-used the Late Paleozoic basement structures and is associated with the Paleogene intra-continental rifting phase leading to the opening of the Upper Rhine Graben that evolved to the south along a major continental transfer zone, called the Rhine-Bresse Transfer Zone (RBTZ, Fig. 1a). This latter is localised by the Late Palaeozoic ENE-striking inherited basement faults. The RBTZ linked the simultaneous opening of the Upper Rhine Graben in the NE and Bresse Graben in the SW by sinistral transtensive reactivation of ENE-oriented basement faults of the pre-existing Permo-Carboniferous trough system (Laubscher 1972, 1973; Bergerat and Chorowicz 1981; Illies 1981; Ziegler 1992; Lacombe et al. 1993). Rifting in the southern Upper Rhine Graben began in the Upper Priabonian and persisted until Late Oligocene to Early Miocene under regional WNW-ESE extension, roughly perpendicular to the graben axis (Pflug 1982). This led to the formation of NNE-trending growth faults delimiting half grabens (e.g. Ferrette half-graben) and numerous associated extensional faults paralleling the southern Upper Rhine Graben. The trend of this set of faults is commonly termed "Rhenish" in the literature. Simultaneously, ENE-trending extensional flexures evolved in the sedimentary cover above reactivated basement faults; this trend is referred to as "Permo-Carboniferous" (Ustaszewski et al. 2005; Ustaszewski and Schmid 2006).

2.2 Overprint of the Late Miocene-Early Pliocene thin-skinned deformation

In the study area, the Folded Jura front is characterised by a significant change of orientation (Fig. 1). From the west to east, it follows an E-W, then an ENE-orientation, and then rotates into a NNE-trending fault zone connecting up the Ferrette fault further north.

Furthermore, the study region is characterised by the NNE-orientated Caquerelle anticline that closes the Delémont Basin westwards (Figs. 1, 2, 3). This unexpected orientation suggests the presence of inherited basement normal faults at depth as suspected by Laubscher (1963a, b). This fault system is considered to dip to the east. The focal mechanism of the M_L 3.7 earthquake that occurred on December 11th 1987 in Glovelier (47.313N, 7.161E) at a depth of 9 km indicates a left-lateral strike-slip fault on a steeply E-dipping fault plane (Deichmann 1990). This fault presents the same orientation as the Ferrette fault located further north. The Ferrette Fault dips to the west and forms the eastern boundary of the Eo-Oligocene Ferrette half-graben. Based on seismic profiles interpreted by Ustaszewski et al. (2005), throw on this faults varies along strike, ranging from ca. 500 m in its central part and decreasing to 170 m in the south, suggesting a termination of the Ferrette Fault in the north-eastern part of the Mont Terri region. Therefore, we consider that the Ferrette fault evolved to the south into a diffuse transfer zone characterised by the superposition of "Rhenish" NNE-trending faults and reactivated ENE-striking Permo-Carboniferous faults.

2.3 Litho- and mechanical stratigraphy

In order to construct cross sections that define the end state of the forward models presented in Sect. 5, a locally valid stratigraphic column that included the thickness of the Mesozoic units was set up using the stratigraphic subdivisions and formation names according to the nomenclature defined by the Lithostratigraphic Lexicon of Switzerland (www.strati.ch). In all figures of this paper, the formations are illustrated by the official colours as defined by the Lithostratigraphic Lexicon. The formation thicknesses in the region of St-Ursanne were adapted after Laubscher (1963a, b) and complemented by the recent borehole BDB-1 for the thicknesses of the Opalinus Clay and Passwang Formation (Hostettler et al. 2017).

Above the basement evidencing some Late Paleozoic clastic sediment, several hundred meters of Triassic limestone, dolomites, marls, and evaporites follow, mark a depositional change from marine to continental environments. The dolomitic marls, dolomites, and evaporites of the Klettgau Formation belonging to the Keuper are the oldest rocks that crop out in the region of St-Ursanne (Fig. 2). During the Early Jurassic, a fully marine environment with successively increasing water depth developed, leading to the formation of calcareous, marly, and argillaceous rocks denoted as the Staffelegg Formation (Reisdorf et al. 2011). Together with rocks of the Keuper, these rocks form the core of the Mont Terri anticline. They are visible at the surface and were mapped in the Mont Terri area by several authors (Laubscher 1963a, b; Freivogel and Huggenberger 2003). The Staffelegg Formation, which reaches a thickness of up to 70 m, is followed by the 130 m thick Opalinus Clay, a monotonous succession of dark argillaceous rocks with some sandy or carbonate-rich facies variations (e.g. Schaeren and Norbert 1989; Bläsi et al. 1991; Wetzel and Allia 2003; Bossart and Thury 2008). Since the beginning of 2014, a continuous

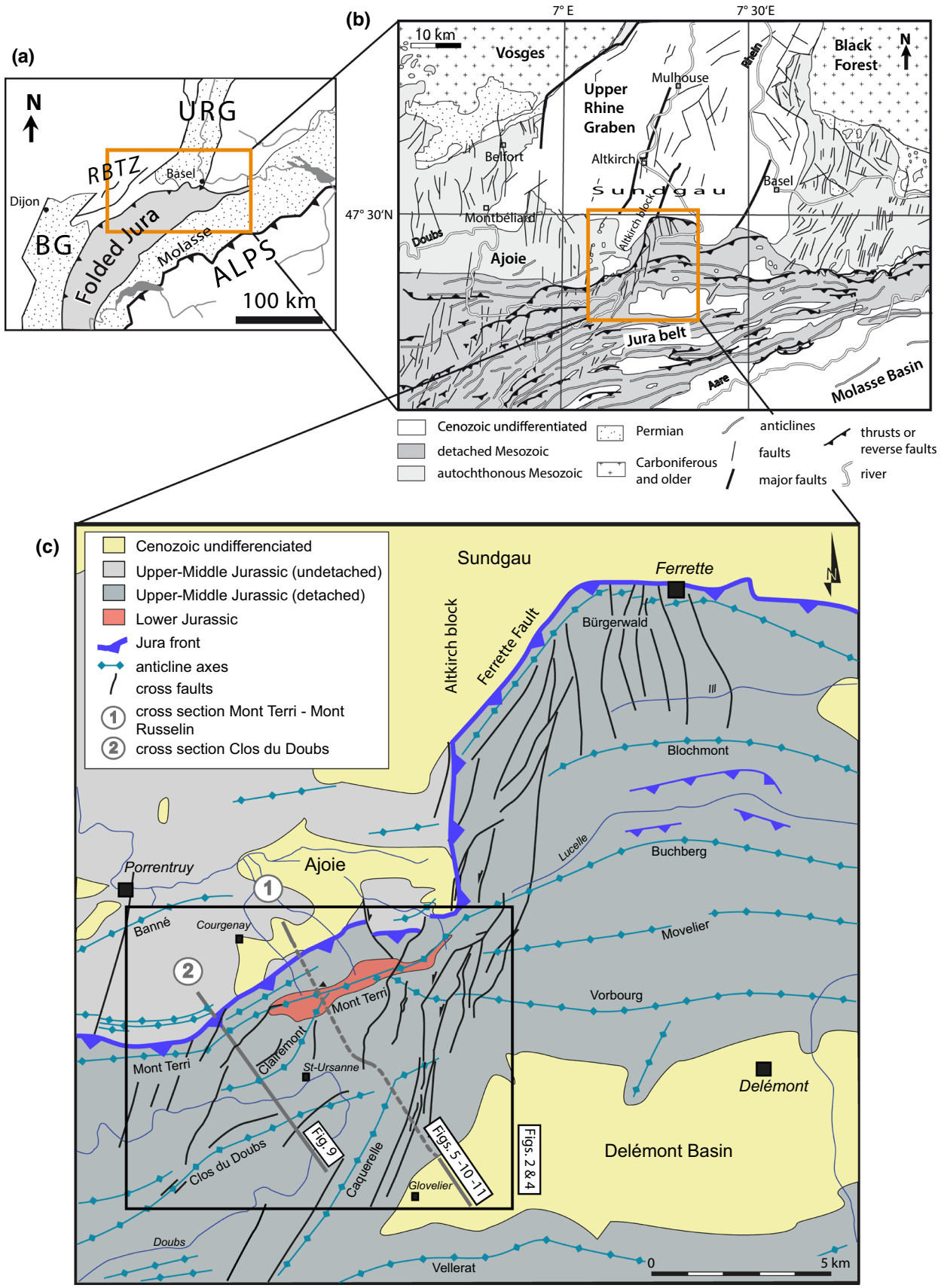
(a)
N
URG
RBTZ
Basel
Dijon
BG
Folded Jura
Molasse
ALPS
100 km
(b)
7° E
7° 30'E
10 km
Vosges
Upper Rhine Graben
Mulhouse
Rhein
Black Forest
N
Belfort
Altkirch
Sundgau
Basel
47° 30'N
Montbéliard
Doubs
Ajoie
Altkirch block
Jura belt
Aare
Molasse Basin
Cenozoic undifferentiated
detached Mesozoic
autochthonous Mesozoic
Permian
Carboniferous and older
anticlines
faults
major faults
thrusts or reverse faults
river
(c)
Cenozoic undifferenciated
Upper-Middle Jurassic (undetached)
Upper-Middle Jurassic (detached)
Lower Jurassic
Jura front
anticline axes
cross faults
cross section Mont Terri - Mont Russelin
cross section Clos du Doubs
Sundgau
Ferrette
Altkirch block
Ferrette Fault
Bürgerwald
Blochmont
Buchberg
Movelier
Vorbourg
Delémont
Delémont Basin
Porrentruy
Ajoie
Banné
Courgenay
Mont Terri
Clairemont
St-Ursanne
Clos du Doubs
Caquerelle
Glovelier
Lucelle
Doubs
Vellerat
Fig. 9
Figs. 5 -10 -11
Figs. 2 & 4
0
5 km

◀**Fig. 1** **a** Tectonic map with the main units of the northern Alpine region. *BG* Bresse Graben, *RBTZ* Rhine–Bresse Graben transfer zone, *URG* Upper Rhine Graben. **b** Large scale tectonic map of the junction between the Jura belt and the Upper Rhine graben. **c** Overview tectonic map of northwestern Folded Jura (modified after Laubscher 1963a, b), with the location of the Mont Terri–Mont Russelin section indicated

geological profile of the Opalinus Clay from the Mont Terri rock laboratory is available from the 250 m deep inclined borehole BDB-1 (Fig. 5). Three main lithofacies types were encountered. From bottom to top, the borehole drilled through 33 m of a shaly facies of Toarcian age with large amounts of bioclastic material followed by 15 m of a shaly facies with many ammonites. The transition to this upper part marks the Toarcian/Aalenian boundary, which was thoroughly biostratigraphically investigated in Hostettler et al. (2017). Further upwards, the borehole encountered 6 m of sandy carbonate-rich facies with several distinct bioclastic limestone beds. At the bottom of this facies, two conspicuous pyrite horizons are present. The carbonate-rich sandy facies is followed by 14 m of sandy facies with a large amount of bioclastic lenses, 35 m of monotonous shaly facies, and an upper sandy facies with marly, sometimes sideritic and sandy nodules. The top of the Opalinus Clay consists of a calcareous hardground with reworked limonitic intraclasts. The next lithostratigraphic unit, the Passwang Formation, is composed of a series of parasequences reflecting a shallow, mixed siliciclastic, and carbonate depositional environment (Burkhalter 1996) with a total thickness of about 70 m. The upper part of the drillhole comprises the Hauptrogenstein, consisting of shallow-water oolitic carbonates with some distinct coral horizons. Gonzalez and Wetzel (1996) described three shallowing-upward successions. These generally start with fine-grained marly beds and end with a maximum flooding surface or a hardground on top of oolitic or sparry bioclastic limestone. The Hauptrogenstein exhibits a total thickness of about 125 m and crops out in the northern overturned limb of the Mont Terri anticline just north of the drilling site. The end of the Middle Jurassic is characterized by shallow-water deposits and iron-oolitic beds of the Ifenthal Formation (Bitterli 2012). The thickness of these deposits is estimated at 55 m in the region of the Mont Terri. It is overlain by deeper-water clays (Gygi 1969) and nodular marls of the Bärschwil Formation, which mark the beginning of the Late Jurassic (Oxfordian). The overlying coral horizons and oolitic limestone with oncoids and patch reefs are remnants of a prograding reefal belt that extended over large areas. Well-bedded platy limestone and oncolithic beds of the Vellerat Formation indicate shallow-water conditions exhibiting a continental influence. Later, a shallow, fully marine carbonate platform evolved and led to the 30 m-thick succession of micritic limestone of the Courgenay Formation. A total thickness of about 250 m can be attributed to the Oxfordian. During the Kimmeridgian, the platform intermittently emerged and water depth varied between 0 and 100 m. Numerous traces of dinosaurs have been found in the micritic and oolitic limestone of the Reuchenette Formation (Marty 2008; Comment et al. 2011).

We identify four levels of relative mechanical weakness that could form potential detachment levels (Fig. 3). The main and basal detachment level occurs within the Middle Triassic evaporites of the Zeglingen Formation. For the forward modelling, we defined the basal detachment as one discrete plane located in the middle of this formation. We realise that this may be an oversimplification and that the detachment may have finite width. A second, less important but still regionally significant detachment, is formed by the bituminous Posidonia shales at the top of the Staffelegg Formation. Drillcore analysis of the BDB-1 borehole (location shown in Fig. 6) revealed a 10 m-thick deformation zone within the Rietheim Member that together with the Gross Wold Member comprises the top of the Staffelegg Formation. We used this horizon as an upper detachment in the forward modelling presented in Sect. 5. In fact, we found no structural evidences in the drillcores and in the galleries for a detachment directly within the Opalinus Clay Formation. Two other minor detachment levels are the relatively weak shales of the Bärschwil Formation and those at the base of the Vellerat Formation. These latter were not used in the modelling for the sake of simplicity. This decision is justified at the regional scale. A model integrating all minor detachments is beyond the scope of this contribution.

3 Observations and existing data

3.1 Constraints from the geological map

The geological map of St-Ursanne (Laubscher 1963a, b) provides an important data source (Fig. 2). Based on the geological map, we present a tectonic map of the same region (Fig. 4). In order to better understand the relationships between the faults and the relief, we have drawn the faults over a hillshade model that illustrates the terrain topography (digital terrain model from Swisstopo 2011). It shows the main structural elements and includes a series of typically ENE-trending anticlinal axial traces mapped mostly as related to thrusts (as hangingwall anticlines), and a set of (N)NE-trending cross faults mostly with sinistral strike-slip component but some with normal displacement. Note the interplay between ENE and NNE-trending anticlinal axes, thrusts, and cross faults, and the

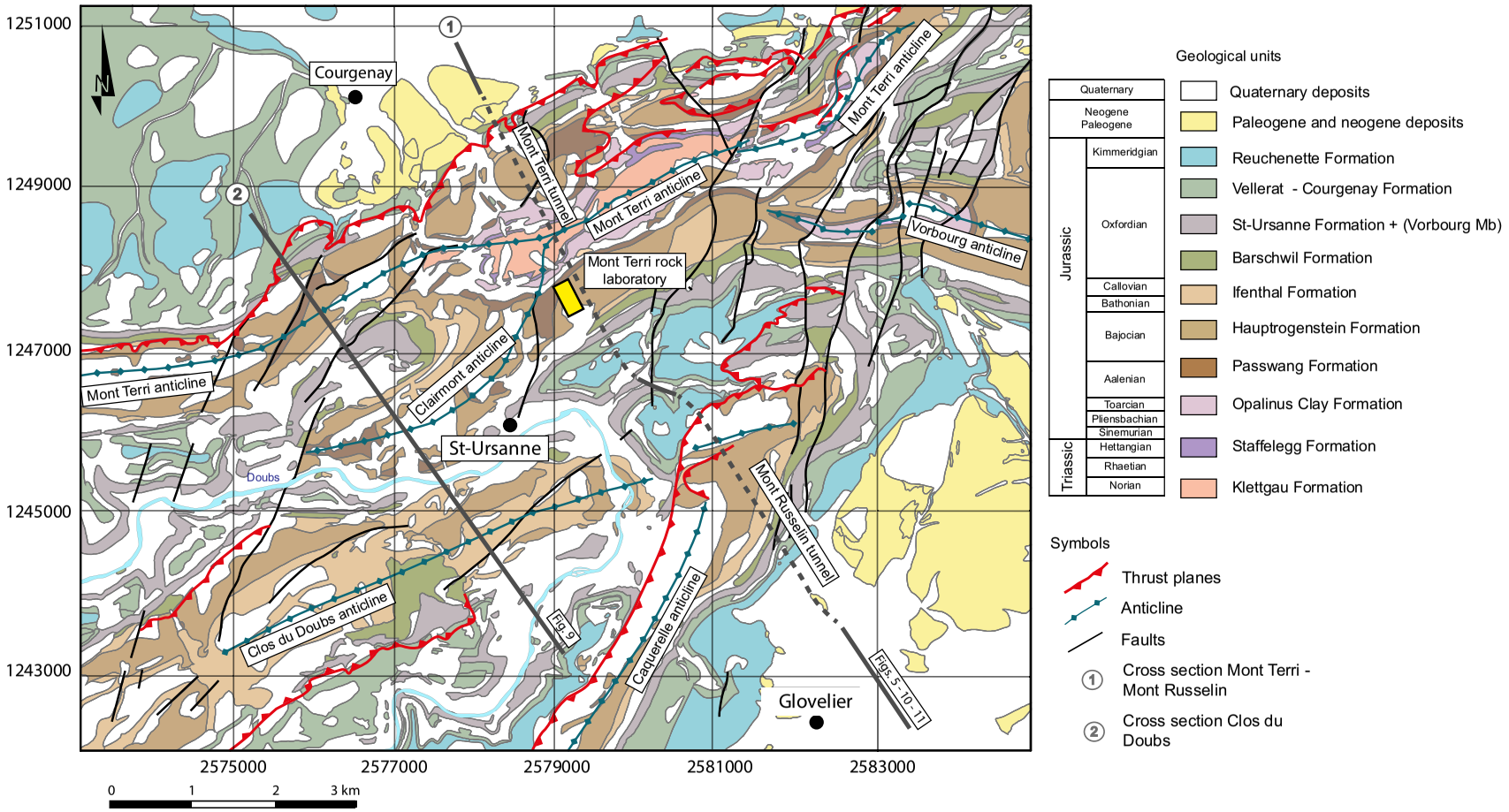

Fig. 2 Geological map of the St-Ursanne area, modified from GeoCover (Swisstopo 2012) and the Geological Atlas 1:25,000 (Laubscher 1963a, b). The formations are illustrated by the official colors as defined by the Lithostratigraphic Lexicon of Switzerland (www.strati.ch). The Paleogene and Neogene deposits encompass the following formations: Conglomerates of Porrentury, Terres jaunes, Meeresand, Septarienton, Alsace Molasse, *Upper* Marine Molasse (marnes rouges & Gompholites), *Upper* Freshwater Molasse (Formation du Bois de Raube, Vogesenschotter). Note the oldest exposed geological unit belongs to the Klettgau formation (Keuper) in the core of the Mont Terri anticline

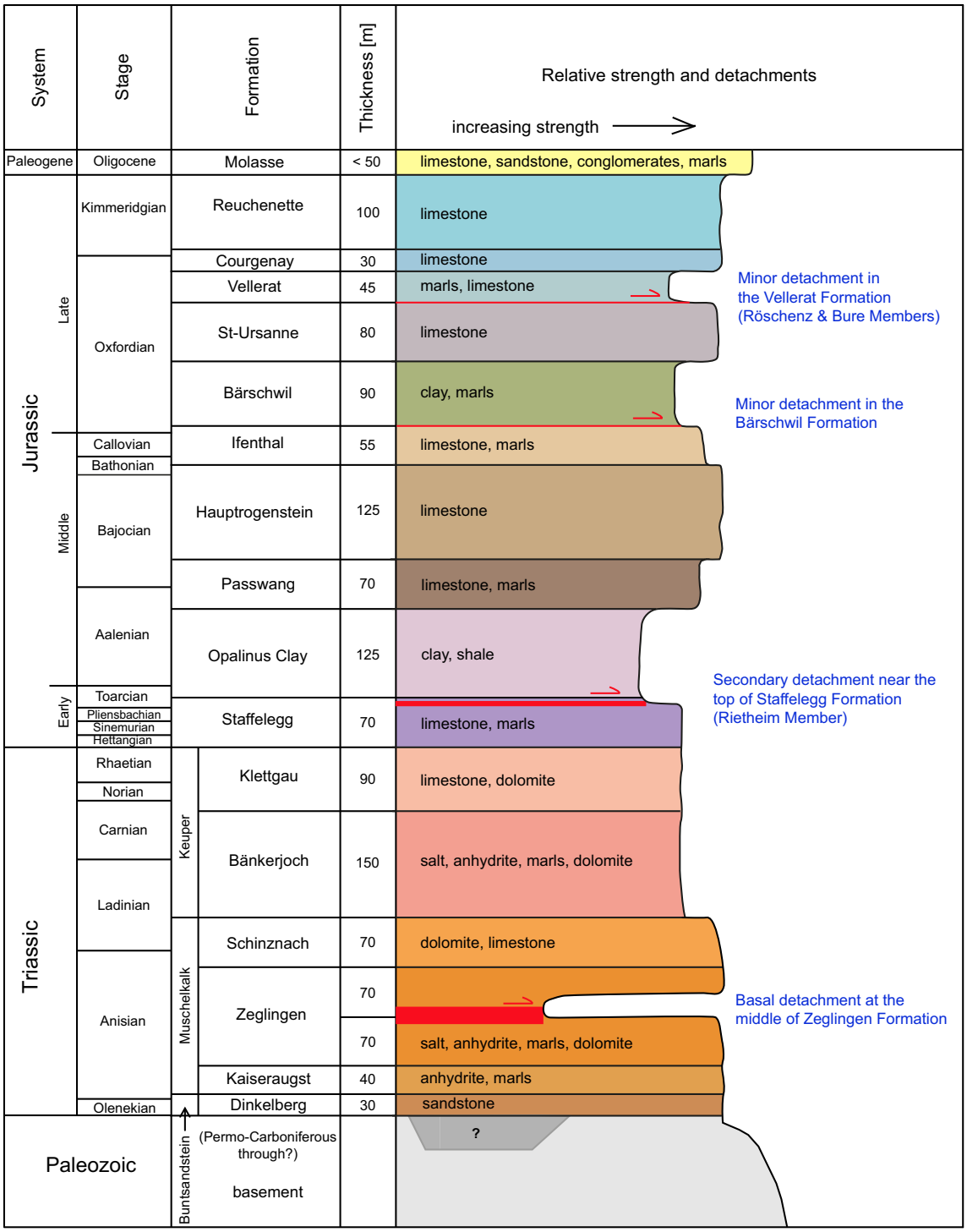

Fig. 3 Compiled stratigraphy of the Mesozoic cover and relative strength and detachments. Thickness of units adapted from Laubscher (1963a, b) and from the Lithostratigraphic Lexicon of Switzerland (www.strati.ch)

intersection with both cross sections presented in Figs. 9, 10, and 11. The anticlines appear to be offset by the NNE-trending thrusts, with complexity added by the Caquerelle anticline that is parallel to the NNE-trending thrust in front.

Most of the NNE-trending cross faults cutting through the anticlines present abrupt variations of the anticlinal traces (Fig. 4, location A). We interpret these faults to have acted as lateral ramps in a sinistrally transpressive mode during the Jura thin-skinned deformation phase. Some of

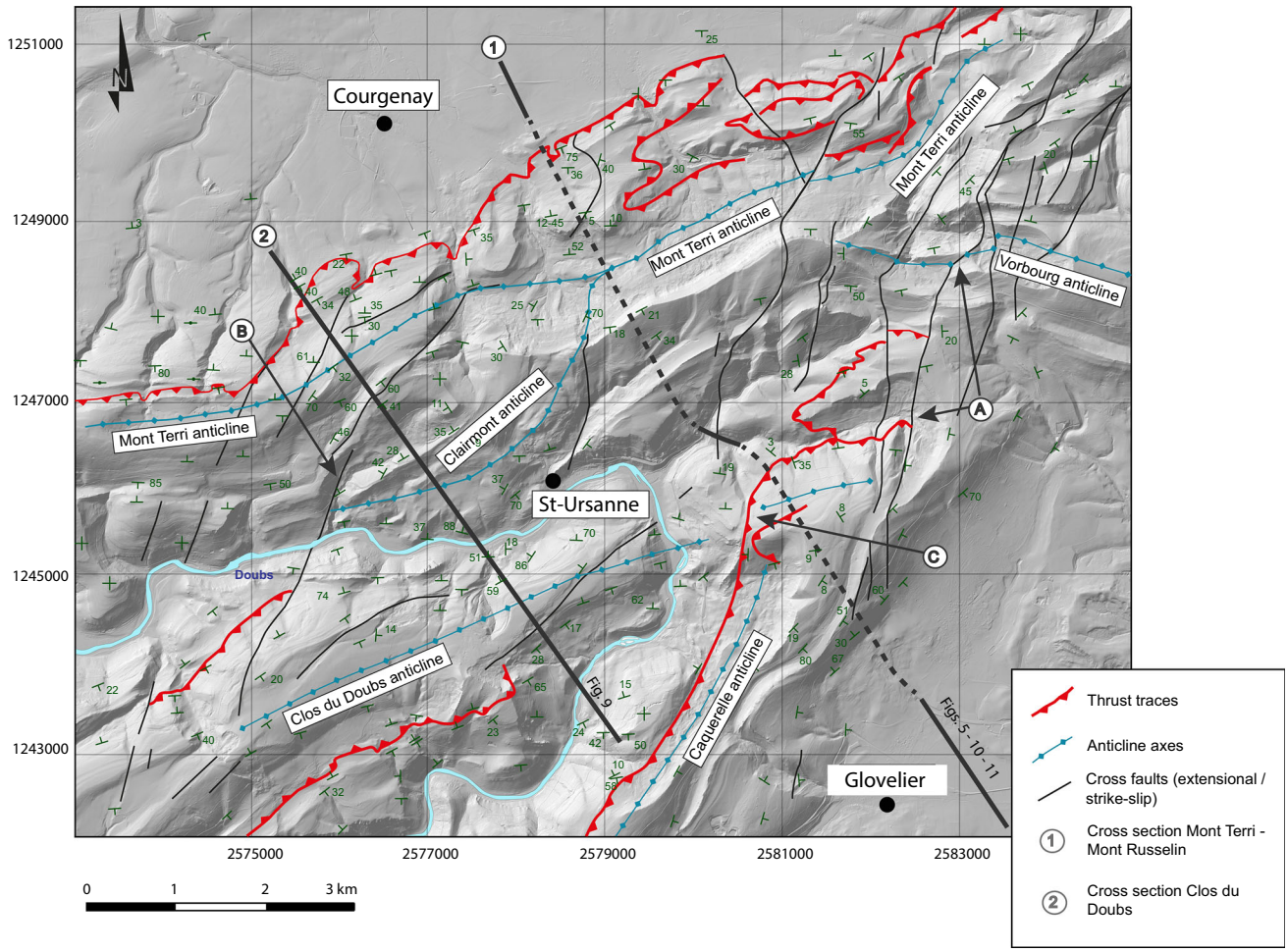

Fig. 4 Tectonic map of the St-Ursanne area, modified from Laubscher (1963a, b). Dip data are taken from Swisstopo (2012). The map overlies a hillshade model that illustrates the topography of the terrain (digital terrain model from Swisstopo 2011). Note the interplay between ENE and NNE-trending anticlinal axes, thrusts, and cross faults, and the intersection with both cross sections. *A* NNE-tending faults typically cut across and sinistrally offset anticlinal traces, *B* NNE-tending faults typically cut across and sinistrally offset anticlinal traces and *C* The La Caquerelle thrust and anticline offsetting the Clos du Doubs anticline and interfering to form the Mont Russelin culmination

the NNE-trending faults have normal components of displacement (Fig. 4, location B). The nature of NNE-trending extensional faults is a subject of discussion, and is addressed in the forward modelling. One of the NNE-trending faults is the Caquerelle thrust. We interpret this thrust to have formed last, cutting obliquely across the ENE-trending folds and thrusts to form the Mont Russelin culmination (Fig. 4, location C). The Mont Russelin culmination is interpreted to be the result of the superposition of two anticlines (ENE-trending Clos du Doubs plunging eastwards beneath the NNE-trending Caquerelle). The NNE-orientation of the Caquerelle anticline, which is unusual in the northern part of the Jura belt, supports formation in situ above an inherited Rhenish basement-rooted fault. In the case of a forward-propagating sequence of the thrust front, this anticline would have been transported further north and the inherited fault that had served as nuclei should be found further to the south, which is not observed on the geological map.

Triassic sediments form the core of the Mont Terri anticline. This is of particular interest because outcrop of Triassic sediments is not common along the trend. This exposure, even if not unique in the Jura belt, may indicate that local structural complexities occurred at depth, which locally uplifted the oldest sediments of the detached Mesozoic to the surface.

3.2 Constraints from tunnel mapping and drillcore observations

In Fig. 5, we present a compilation of all available data from the Mont Terri and Mont Russelin tunnels along a cross section that will serve as a basis for the forward models described in Sect. 5. The data consist of geological

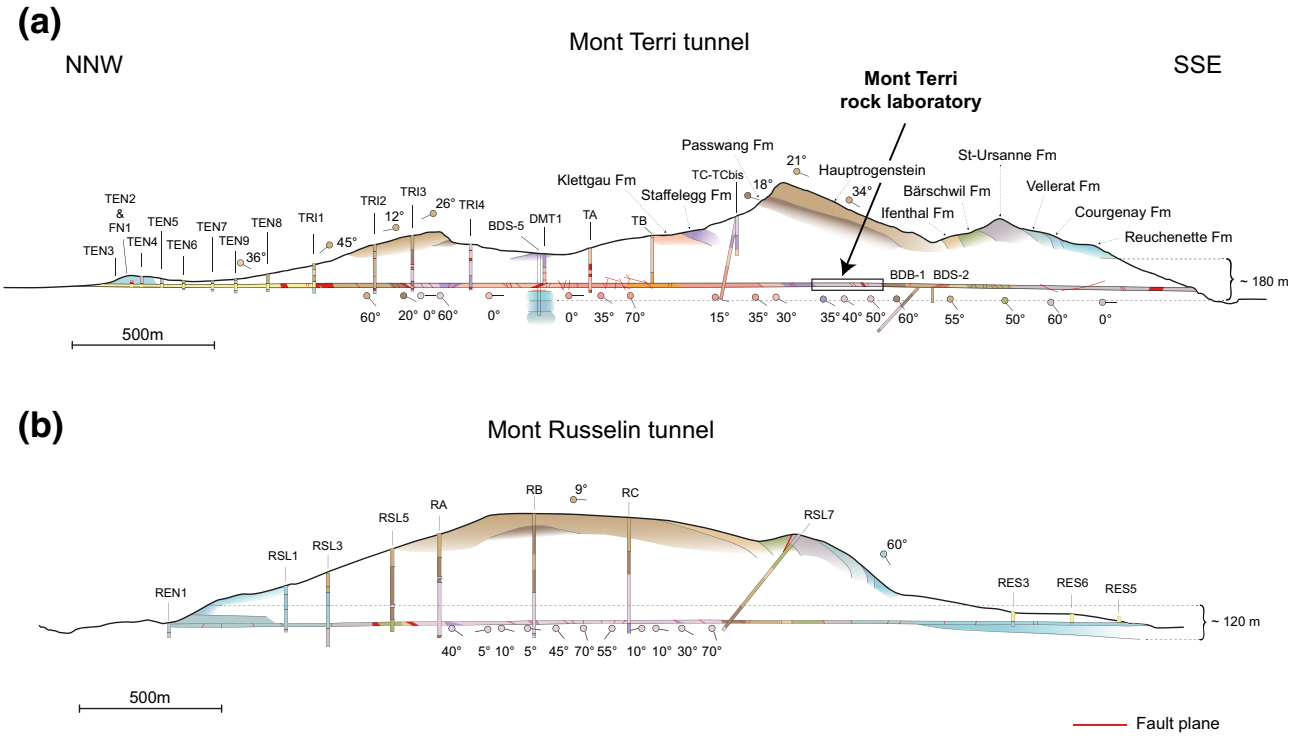

Fig. 5 Sub-surface cross section along the Mont Terri tunnel (**a**) and Mont Russelin tunnel (**b**). Compilation of field data acquired during the excavation of both tunnels and from the drillcore mapping of reconnaissance boreholes by Bureau Technique Jean Norbert Geologues SA (1992), Bureau Technique Norbert Geologues-Conseils SA (1993), respectively. Surface data are taken from GeoCover (Swisstopo 2012). Site map of both tunnel from swisstopo (**c**). Mapped underground fractures in *red*

documentation of reconnaissance boreholes drilled and cored for the construction of the Mont Terri and Mont Russelin tunnels, geological mapping from excavation of both tunnels (Bureau Technique Jean Norbert Géologues SA 1992; Bureau Technique Norbert Géologues-Conseils SA 1993), and surface data from the geological map shown in Fig. 2. We have also integrated key boreholes (i.e. BDS-5, BDB-1 und BDS-2) drilled in the framework of the Mont Terri research programme (i.e. Jaeggi and Bossart 2016; Hostettler et al. 2017). Stratigraphic and structural constraints, with dips and dip azimuths of bedding and structures, were taken from the tectonic map (Fig. 4) and projected onto Fig. 5.

The main structural observations constraining the forward modelling include (also refer to Sect. 5):

- The structural level of the stratigraphic sequence in the hangingwall syncline between the Mont Terri and Caquerelle anticlines, taken to indicate a relative uplift

of stratigraphy of ca. 180 m compared to the footwall and the presumed regional and reference level to the north in the Ajoie plain. Any forward model will need to explain this locally elevated level.
- The conspicuous subhorizontal fault, the shallow-dipping Mont Terri thrust, that surfaces near the northern entrance of the Mont Terri tunnel and that separates the strongly folded hangingwall from the flat-lying and largely undeformed footwall;
- The strongly folded and locally overturned nature of the hangingwall of the Mont Terri anticline.
- The backlimb of the Mont Terri anticline that presents a mean dip of 30° to the SSE. However, in the vicinity of NNE-trending cross faults, the strata are steepened and plunge with larger dips (50°–60°). For the forward modelling, we applied the mean dip and for the present ignored the local perturbations, because they are likely to result from a different set of structures.
- The structural level of the stratigraphic sequence in the hangingwall syncline between the Mont Terri and Caquerelle anticlines is taken to indicate relative uplift of stratigraphy of ca. 120 m compared to the hangingwall and presumed regional and reference level to the south in the Delémont Basin close to Glovelier. A 2° dip of the basement surface to the SE enables us to explain the level difference of the stratigraphic sequence without invoking any basement bump.
- The stratigraphic and structural constraints, applied taking dips and dip azimuths of bedding and structures from the map, and projected onto the sections.

Figure 6 illustrates a subsurface cross section around the Mont Terri rock laboratory. This section integrates all available geological data from the Mont Terri tunnel and the relevant boreholes to define the stratigraphic formation boundaries. The different galleries of the Mont Terri rock laboratory, as well the security and Mont Terri motorway tunnels, are all intersected by a second-order thrust zone (1.0-to-4.2 m thick), called "Main Fault". Close observation and structural analysis of outcrops in the galleries suggest that the Main Fault formed as a simple-shear fault-bend fold (Nussbaum et al. 2011). The beds of the hangingwall dip less than the fault ramp, which is in this case the shear-zone boundary, dipping 50°–60° SSE. The angular difference of beds between the footwall (30°–35°) and the hangingwall (40°–45°) ranges from 10° to 15°. These geometric relationships favor an interpretation as a shear fault-bend fold (Suppe et al. 2004), in contrast with a classical fault-propagation fold or fault-bend fold where backlimb dips are parallel to the fault ramp.

4 Methodology

4.1 Kinematic forward modelling

4.1.1 Methodology and workflow

Two sections, one through the Mont Terri and the Mont Russelin tunnels, and one through the Clos du Doubs area, were set up in 3D digital space using Move™ (see Fig. 2). Even though the section construction and kinematic analyses were done in 2D, it was important to analyse the sections in the 3D context of a regional Digital Elevation Model (swissALTI3D, Swisstopo 2011) with draped geological maps (Geological Atlas, GeoCover, swisstopo), since this provided context and additional constraints on bedding and fault geometry, particularly faults that were not at right angles to the section. First-order faults that crossed the sections were constructed as 3D wireframes from a selection of planar fault segments, constructed by solving local three-point-problems constrained by surface trace geometry and topography. The section interpretation was extended to depth by iterative kinematic forward modelling following the two end-member concepts to be tested (see Sect. 4.1.2).

We performed kinematic forward modelling of deformation, including folding and faulting, using Move™. This software provides a range of algorithms that mimic rock deformation styles including algorithms for fault-bend folding (Suppe 1983), and fault-propagation folding (Suppe and Medwedeff 1990) and Trishear (Erslev 1991). Kinematic forward modelling goes beyond the traditional line-length and area-balancing tests in 2D and 3D by including constraints on the sequence of deformation events and the mechanism by which deformation took place. As such it allows testing and quantification of not only the deformation style but also the order of faulting through time, and the geometry of horizons and faults at sequential steps in time. It is of particular use in data-poor studies where sequential restoration is under-constrained.

Typically, forward modelling is an iterative process where forward-modelled geometries are compared and contrasted to observed geometries and cross-cutting relationships, and modelling variables are adjusted accordingly.

Our approach comprised the following steps with the iterative process visualised in Fig. 7:

1. Data Integration: we took existing sections by Freivogel and Huggenberger (2003) and Caër et al. (2015) as a starting point, organized available field-, tunnel, and drilling data and interpretations, and integrated in 3D georeferenced space including maps of various vintages, topography, and additional sections.

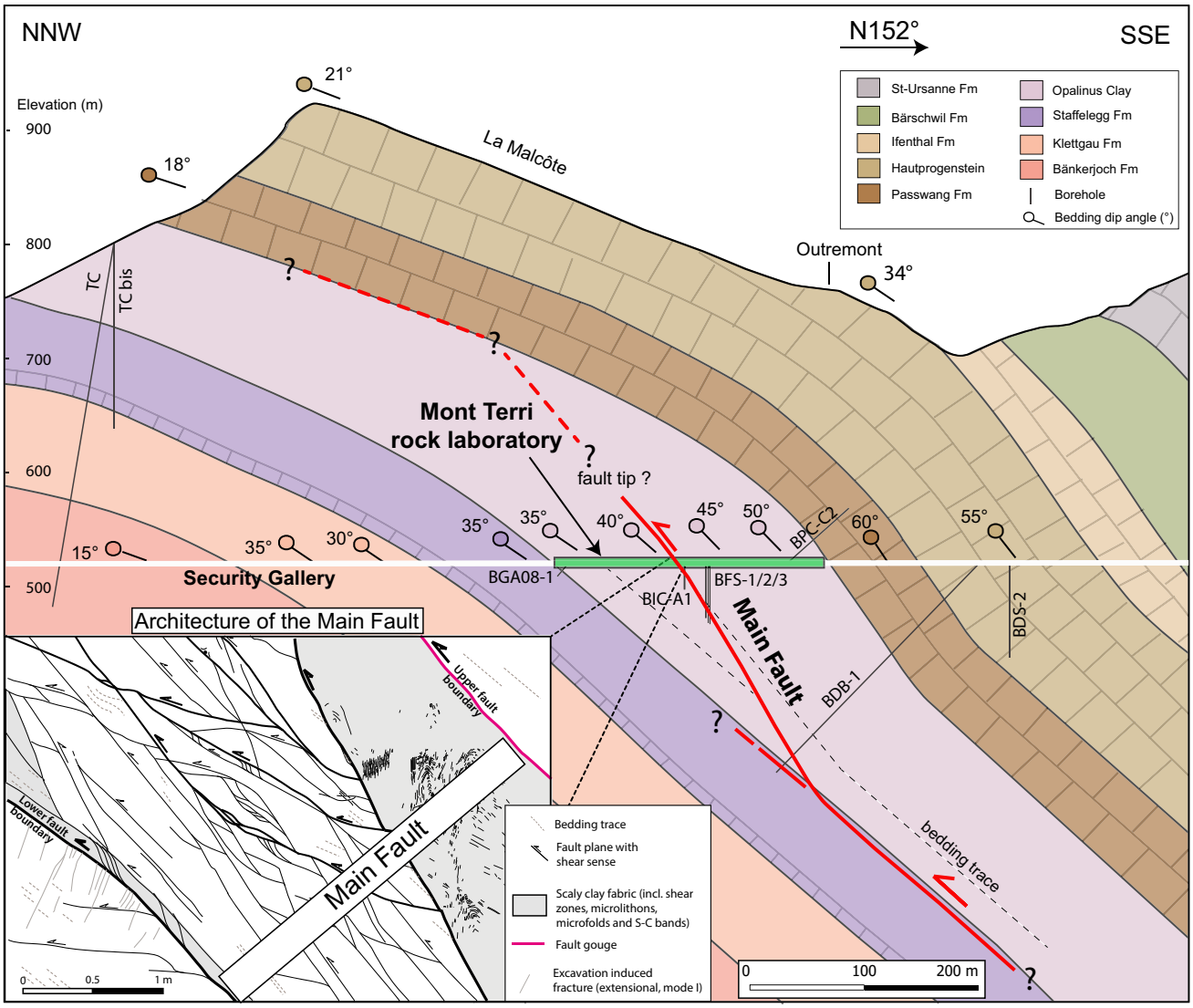

Fig. 6 Sub-surface cross section based on tunnel and borehole data collected within and in the vicinity of the Mont Terri rock laboratory. The main tectonic structure intersecting the rock laboratory is the 1–6 m wide "Main Fault'' and is described in Nussbaum et al. (2011) and Jaeggi et al. (2017). The significance of the fault for this study is that it is considered as being detached from the upper detachment at the top of the Staffelegg Formation. Surface data are taken from GeoCover (Swisstopo 2012)

2. First-pass observations and structural constraints (described in Sect. 3) then led to an extrapolation of the interpretation of faults and fault block geometries to depth, following the two structural concepts to be tested.
3. Forward modelling then tested these first-pass geometries by applying fault displacements starting with a layer-cake stratigraphic sequence including a regional tilt.
4. For both scenarios, we identified the key modelling variables, determined the sensitivity of the results to the various settings, compared the resulting geometries and contrasted these with near-surface constraints, and selected an optimum set of parameters for each scenario (listed for each scenario in Sect. 5.2, Fig. 8).

The final iteration of our (re-)interpretations led us to select one optimum scenario (described in Sects. 5.2, 5.3, and visualised in Figs. 10, 11).

4.1.2 *Initial boundary conditions and modelling constraints*

We chose the section through the Mont Terri and Mont Russelin tunnels because of the abundance of available data acquired by the geological mapping of the fresh outcrops in both tunnels. Our section trace is not straight but steps in order to connect the trajectories of both tunnels as shown in Figs. 1 and 2. The dog-legged section is "rolled-out" to work in 2D view; this preserves the line length

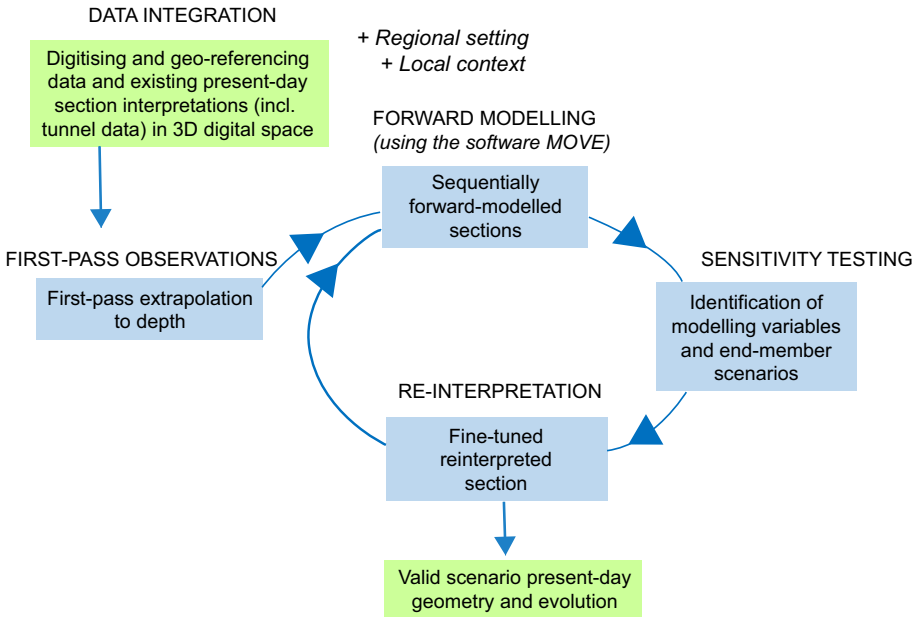

Fig. 7 Kinematic forward modelling workflow with iterative steps, using first-pass extrapolations to depth as target geometries in the sequential forward modelling. Modelling variables and tested scenarios are shown in Fig. 8

going from the section in 3D to 2D, but may lead to overestimating length in a particular transport direction. During the ongoing analysis, we found that part of the late development involved tectonic transport that was not parallel to the Mont Terri section. This meant that the forward modelling in 2D for this particular step was limited. As such, we could not produce all geometries purely by using deformation algorithms. This is further discussed below in Sect. 5.

We assumed stratigraphic thicknesses to be constant for the units on top of the basement and on top of the post-Permo-Carboniferous sediments, even though the presence of mechanically weaker units are expected to have formed local, second, or third order structural duplications and/or omissions. We also assigned a general pre-folding SSE regional tilt for the stratigraphic sequence with a 2.0° instead of a 2.5° dip (Laubscher 2003). This decision was motivated by analysis of the reflexion seismic lines 73-BE5 and 74-BE10 acquired in 1973 and 1974 by Jura Bernois Pétrole SA, partly published by Suter (1978). These seismic lines show that the main stratigraphic horizons plunge to SSE with a dip of 2.0°.

As described in Sect. 3.1, we took the structural level of the stratigraphic sequence in the hangingwall syncline between the Mont Terri and Caquerelle anticlines to indicate relative uplift of stratigraphy of ca. 180 m compared to the footwall and presumed regional and reference level to the north in the Ajoie plain. This structural high is an important geological constraint and we integrated this as an initial condition in the forward modelling. Such local uplifts can be tentatively related to at least three different tectonic styles: (1) presence of inherited basement normal faults creating a basement topographic high in the form of a horst (i.e. Guellec et al. 1990), (2) partial duplication of the Mesozoic sedimentary sequence along an upper detachment as proposed by Schori et al. (2015), or (3) thick-skinned tectonics involving fault reactivation and the creation of basement ramps as proposed by various authors for different regions in the Jura belt (i.e. Guellec et al. 1990; Pfiffner et al. 1997). In the study region, there were no available field data on the basement structure below the Mont Terri and Caquerelle anticlines to allow us to prefer one tectonic style over the other ones.

Considering the regional tectonic setting and available seismic data further north in the Ferrette half-graben (Rotstein et al. 2005; Ustaszewski et al. 2005; Ustaszewski and Schmid 2007), we favoured the presence of inherited basement normal faults and a horst to construct our generic model (Fig. 10). As initial boundary conditions, we assumed that the level difference (+180 m) between the Ajoie Plain and St-Ursanne is related to the presence of NNW-dipping normal faults lowering the basement below the future position of the Mont Terri anticline. We interpreted these as inherited Permo-Carboniferous faults. It is not clear if these inherited faults have also affected the sedimentary cover or not. Certain steep faults observed in the geological map (Fig. 2) could be interpreted as pre-existing normal faults formed during the Oligocene rifting phase. The available geological data along the Mont Terri and Mont Russelin tunnels are not convincing enough to introduce inherited normal faults dissecting the sedimentary sequence at the initial stage (see later below Fig. 10, step 1). For this reason, in setting up the model we assumed a NNW-vergent flexure of the sedimentary cover (and no

cross-cutting of the sediments) above suspected inherited basement faults. Furthermore, we questioned the presence of an eventual Permo-Carboniferous trough north of the section below the Ajoie plain. This possibility has already been addressed by Ustaszewski et al. (2005). Recent unpublished gravimetric data acquired by Geo-Energie Suisse AG for the geothermal project Haute-Sorne also suggest an important negative Bouguer anomaly below the Ajoie plain. Even if there are no available data, such as subsidence curves, we envisaged differential compaction in addition to extensional faults to explain the postulated NNW-vergent flexure. We did not introduce any additional basement fault south of the section to explain the stratigraphic difference level between St-Ursanne and Glovelier (−120 m) as shown in Fig. 5. The unpublished E-W-oriented seismic line 74-BE10 suggests the presence of two E-dipping faults affecting the Mesozoic sedimentary sequence and the pre-Triassic basement. There are also the Develier and Viques faults located further to the east of the Delémont Basin. By contrast, due to the poor resolution of this seismic line, we could not identify any basement fault below the Caquerelle anticline. This justified our decision to use the general 2.0° basement tilt to the SSE to explain the altitude difference.

The alternative scenario involved a partial duplication of the sedimentary sequence. In this model, we assumed a flat topography of the basement surface (see later below Fig. 11, step 1). This model does not imply the absence of basement faults but rather that they create no significant offsets within the sedimentary units.

5 Kinematic forward models

5.1 Modelling variables and proposed scenarios

We tested iteratively both classic and alternative scenarios for the section interpretations: the classical scenario with the basal detachment at Triassic evaporites level, and the alternative scenario in which displacement was on combined detachments within the Triassic evaporites and top of the Staffelegg Formation that led to the partial duplication of the sedimentary sequence. We considered the following five modelling variables (see Fig. 8).

1. Dip angles: the stratigraphic sequence was set up with a 2° regional tilt towards the hinterland. We constructed thrust-ramp angles at 25° (apart from those of the Caquerelle thrust, which are expected to be steeper due to their interpreted nature as sidewall ramps with oblique slip displacement; these are drawn with a 60° angle, an apparent dip because of the section angle).
2. Sequence of thrusting: we varied this to test whether a simple in-sequence order would suffice to explain the observed geometries.
3. Active detachment level(s) and linkages of detachments: we tested whether one single detachment level, or a combination of detachments levels with duplication of part of the sequence, are possible. We know what the dominant regional detachment is; in addition, we know which theoretically weaker stratigraphic units can be expected to have formed additional detachments.
4. Dominant representative deformation algorithm(s): the "duplication scenario" used fold-bend-folding as the dominant deformation algorithm, the "classical scenario" used the Trishear algorithm (Erslev 1991; Allmendinger 1998) for the main displacement. Both scenarios relied on the use of the Trishear algorithm (Erslev 1991; Allmendinger 1998) to produce the overturned frontal limb of the Mont Terri Anticline.
5. Role of basement structures in the initiation of thrusts, development of the local high in the Mont Terri hangingwall, and lateral (dis)continuity of thrusts and folds: we will discuss both scenarios below.

5.2 Lateral structural variability

The large lateral variability of structures, such as significant variations of anticline axes and thrust orientations as observed on the map in Fig. 4, require 3D analyses that will be realised in the future. For this study, we have built an additional cross section to the west of the main section (labelled 2 in Figs. 2, 3), intersecting the Clos du Doubs anticline (Figs. 8,9). The aim of this section is to verify if the same thrust sequence can be derived as that from the main section (Figs. 10, 11), and to understand how the structures evolved laterally and interfere with each other. The forward model presented in Fig. 9 suggests an out-of-sequence order of thrusts. This sequence comprises (1) ca. 90 m displacement due to pre-thrusting normal faulting in the Oligocene rifting phase (Fig. 9, step 2), (2) 100 m displacement due to fault-bend folding and 400 m trishear together comprising the Mont Terri thrust displacement (Fig. 9, step 2), (3) 700 m + 500 m of fault-bend folding with back-stepping of deformation and initiation of two wedges: Clairmont (Fig. 9, step 3) and Clos du Doubs (Fig. 9, step 4). The overturned limb of the Mont Terri anticline required that we add 400 m trishear displacement implying an important bed-thickness change. The hangingwall of the Mont Terri anticline (Fig. 10, step 4) is affected by important NNE-trending faults marking the spot where the E-W trend changes to NE (Fig. 4). This suggests that the NNE-trending faults are cross faults

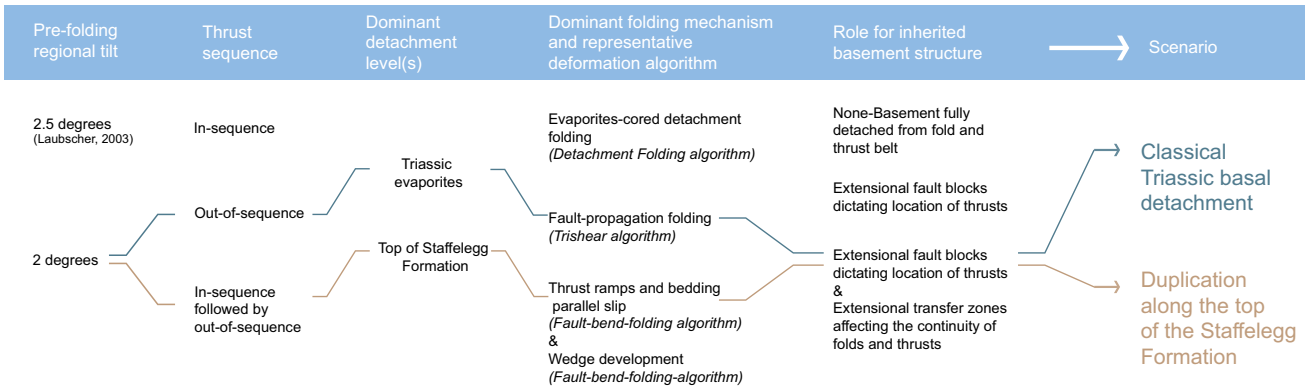

Fig. 8 Forward-modelling variables, range of considered options for each variable, and selected options for the two alternative scenarios that are considered in this study

accommodating sinistral NNE-displacement and causing an out-of-section displacement. We interpret these cross faults as inherited normal faults reactivated during Eo-Oligocene rifting. A pre-thrusting displacement of ca. 90 m is implemented (Fig. 9, step 1). This is in accordance with the amount of throw along the Eo-Oligocene faults estimated by Ustaszewski et al. (2005) to be on the order of 80–90 m based on the interpretation of seismic profiles located further north. We estimate the total shortening accommodated along the whole section to be 2.7 km.

5.3 Scenario with classical basal detachment

5.3.1 Thrust sequence

The cross sections shown in Fig. 10 illustrate our geological interpretation of first-order structures observed in and around the Mont Terri and Mont Russelin tunnels. We have integrated data from mapping of both tunnels and from surrounding reconnaissance boreholes drilled in preparation for the tunnel construction (Bureau Technique Jean Norbert Géologues SA 1992; Bureau Technique Norbert Géologues-Conseils SA 1993). For the purpose of this modelling study we considered only first-order thrusts and faults in the cross section.

We found that a thrust sequence propagating purely forward from south to north to be inconsistent with the cross-cutting relationship as interpreted from the tectonic map (Fig. 4). An in-sequence thrust sequence failed to reproduce the present-day geometry of the geological data compiled in Fig. 5. After several iteration runs, it became clear that the folds and thrusts of the Mont Terri anticline developed first (Fig. 10, steps 2, 3 and 4), followed by those of the Clairmont anticline (visible only in Fig. 9) and the structures of the Clos du Doubs (Fig. 10, step 6). The Mont Terri thrust developed initially with 900 m displacement as fault-bend fold (Fig. 10, step 2). The

Fig. 9 Forward-modelled cross section of the Clos du Doubs to constrain and validate the thrust sequence of the forward models for the Mont Terri–Mont Russelin section (Fig. 10). Section trace is shown in Figs. 1, 2, and 4. Initial basement-related extensional faults are offset by an out-of-sequence series of thrust-wedges that connected the basal detachment to the detachment in the overlying Staffelegg Formation to form a tectonic wedge and a presently surfacing back-thrust. The final-stage geometry shown under (4) was not modelled in detail to fit with the present-day geometry. The stratigraphic units are described in Figs. 2 and 3

observed overturned forelimb formed during trishear development of the Mont Terri anticline (Fig. 10, step 3). The Mont Terri thrust comprises a master thrust associated with smaller thrusts in the hangingwall. These smaller thrusts are folded because of progressive displacement on the master thrust (Fig. 10, step 4).

The Clos du Doubs thrust followed the development of the Mont Terri thrust (Fig. 10, step 6). This thrust also detached along Triassic evaporites but rather than cutting across to the surface, it connected to the top of the Staffelegg Formation to form a wedge that, paired with the associated backthrust, jacked up and folded the overlying units (Fig. 10, step 6). Prior to forming the wedge, the thrust propagated to the north and the Main Fault (as observed in the Mont Terri rock laboratory) developed in the hangingwall as a second-order structure detaching within the top of the Staffelegg Formation (Fig. 10, step 5).

A pair of thrusts developed on the back of the Clos du Doubs wedge (Fig. 10, steps 8 and 9). Similar to the Mont Terri thrust, these connected the Triassic evaporite detachment to the surface, but they show complex deformation at the top of the Staffelegg Formation level as well. Offsets of the deeper units are larger than those of the younger overlying units. The 60°–80° dip of these thrusts is unusually steep for thrust structures. Also, these structures trend NN at the surface and comprise part of the Caquerelle fault exhibiting a “Rhenish” trend. This suggests an

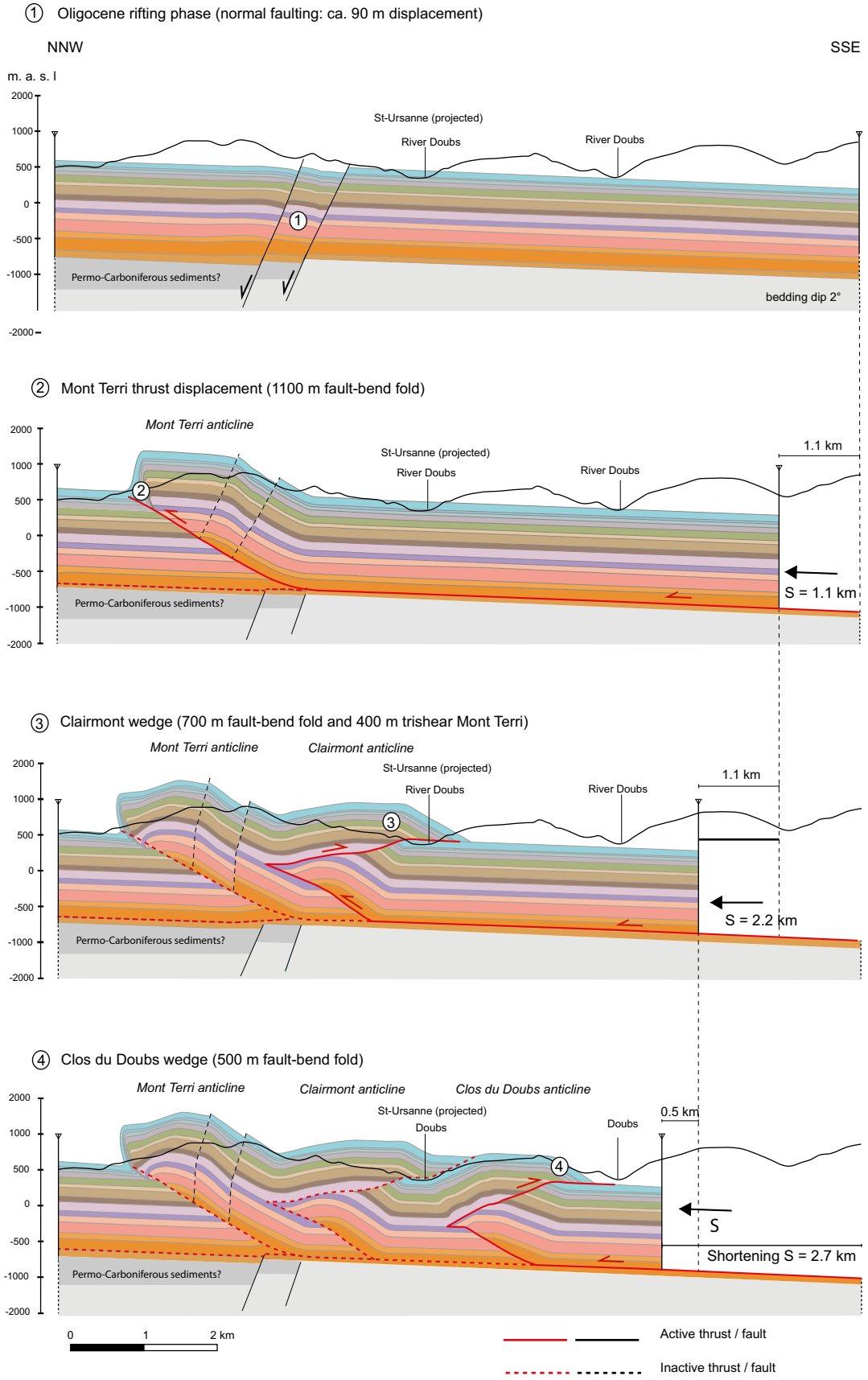
① Oligocene rifting phase (normal faulting: ca. 90 m displacement)
NNW
SSE
m. a. s. l
2000
1000
500
0
-500
-1000
-2000
St-Ursanne (projected)
River Doubs
River Doubs
Permo-Carboniferous sediments?
bedding dip 2°
② Mont Terri thrust displacement (1100 m fault-bend fold)
Mont Terri anticline
1.1 km
S = 1.1 km
③ Clairmont wedge (700 m fault-bend fold and 400 m trishear Mont Terri)
Mont Terri anticline
Clairmont anticline
S = 2.2 km
④ Clos du Doubs wedge (500 m fault-bend fold)
Mont Terri anticline
Clairmont anticline
Clos du Doubs anticline
Doubs
0.5 km
S
Shortening S = 2.7 km
0
1
2 km
Active thrust / fault
Inactive thrust / fault

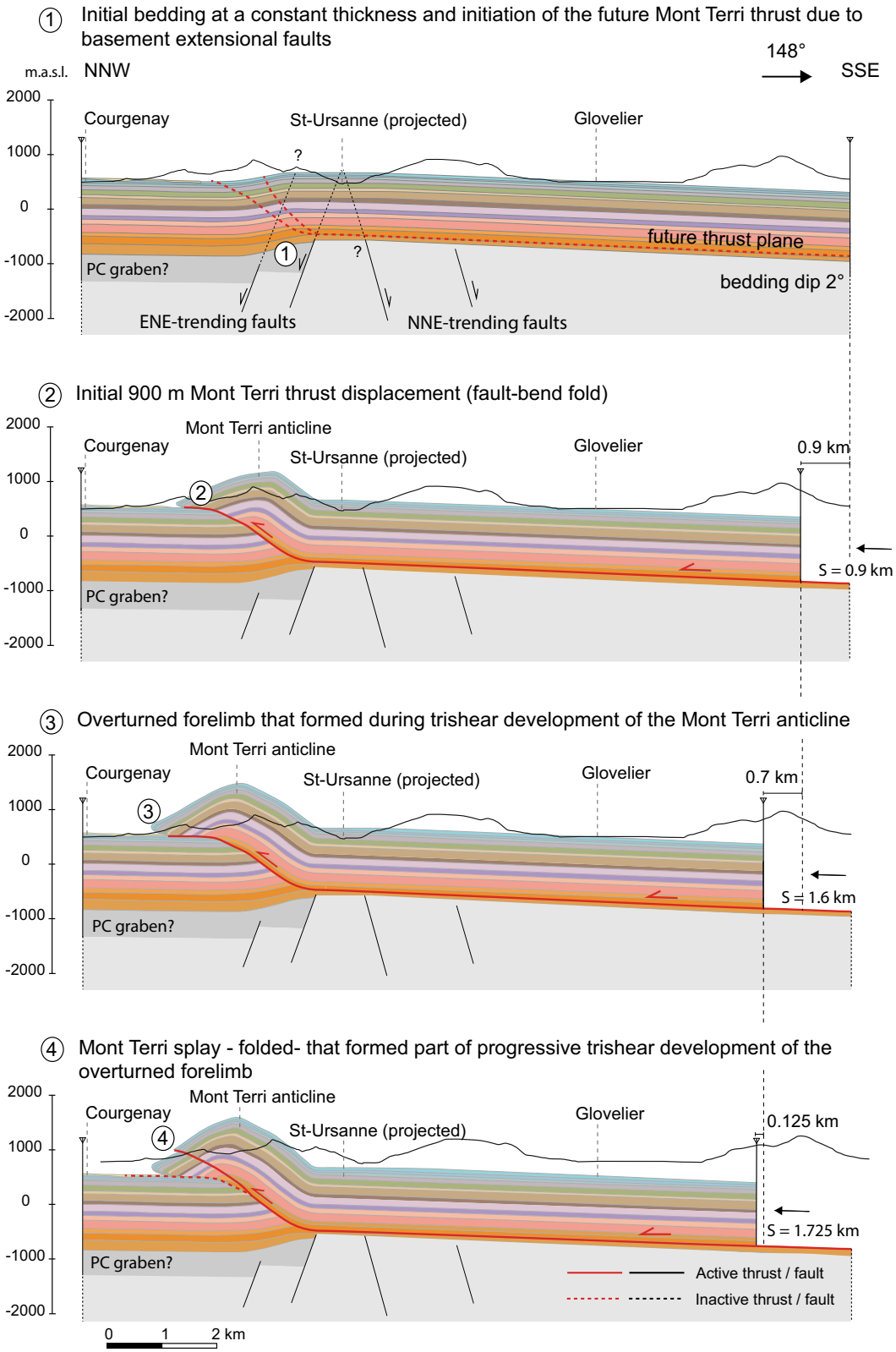

Fig. 10 Forward-modelled cross section of the Mont Terri and Mont Russelin using the classical scenario with a basal detachment. The syncline that is above regional between Mont Terri and Clos du Doubs anticlines relies on a local high formed by a basement horst. The initial Clos du Doubs anticline is formed by a thrust wedge (like in the Clos du Doubs section, see Fig. 9), but is enhanced by a series of NNE-trending steep thrusts. Section trace is shown in Figs. 2 and 4 and stratigraphic legend from Figs. 2 and 3

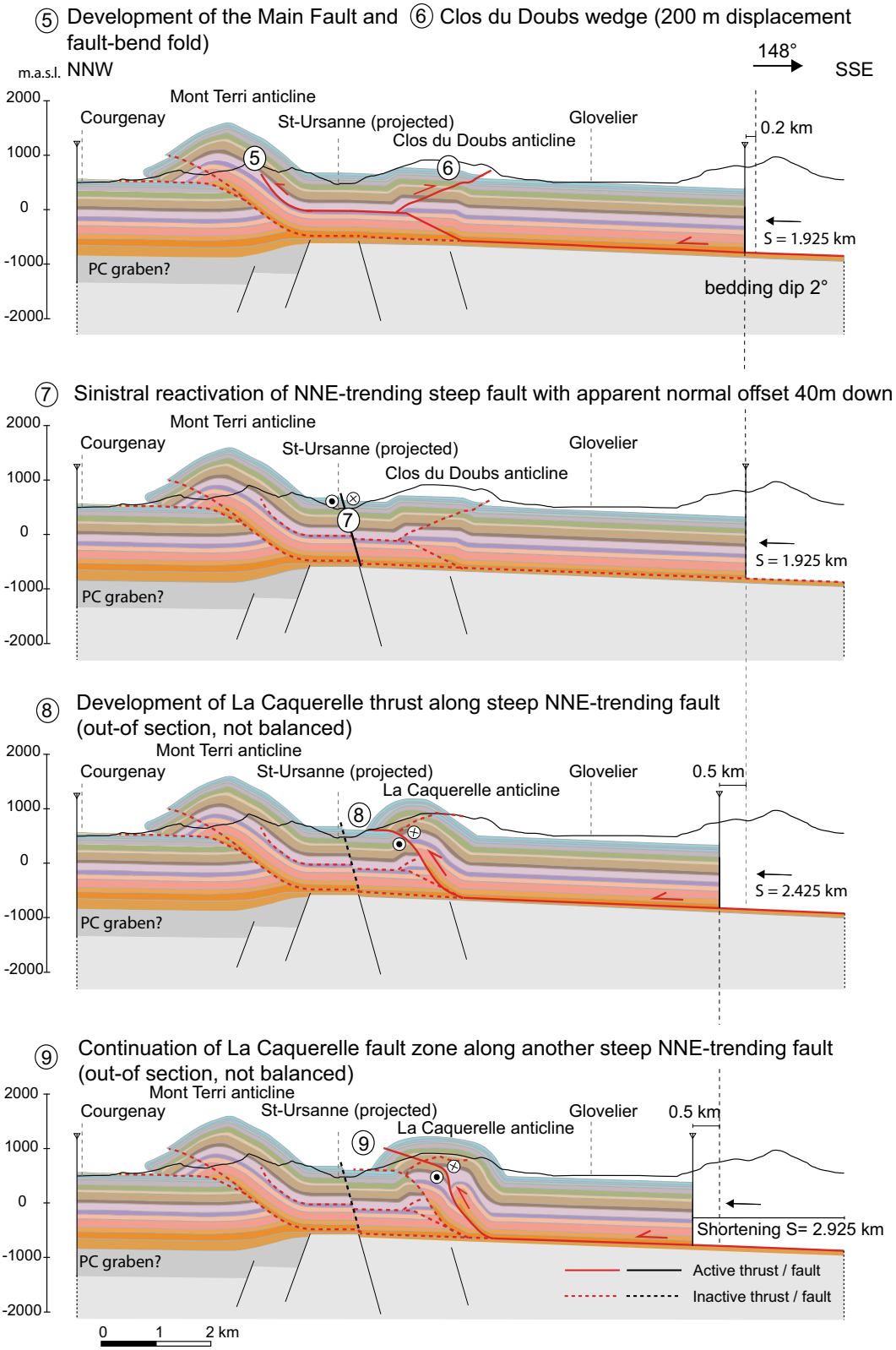

Fig. 10 continued

influence from basement faults in determining their location and geometry. The Caquerelle fault is interpreted to have acted as a sidewall ramp and have a significant oblique slip component that adds complexity to calculating the displacements. For our section, this is an out-of-plane tectonic transport, potentially causing offsets to be apparent offsets and limiting the use of the kinematic modelling algorithms.

One fault in the centre of the section shows normal offset (Fig. 10, step 7). It is interpreted as an isolated steep fault related to a possible underlying basement fault. The actual displacement or kinematics is unknown. Its timing is unconstrained by overprinting relationships with the thrusts.

5.3.2 Folding mechanism

The first 900 m displacement on the Mont Terri thrust was modelled with a fold-bend-fold algorithm, in which the development of the hangingwall anticline follows purely from the shape of the underlying fault (Fig. 10, step 2). The subsequent 1600 m offset was modelled with a Trishear algorithm, which combined discrete offset along the fault at depth with folding in a triangular zone near the surface. A trishear zone with a 30° angle was used with the lower side parallel to an erosional intra-Reuchenette surface (at 2° dip to SSE), which, combined with a small (0.1) propagation/slip ratio, caused the subtle overturned frontal limb with overturned angles reflecting those measured in the youngest units in outcrop today (Fig. 10, step 3). At that stage, is was likely that the flat-lying Mont Terri thrust had become less favourable for slip, and that the small thrust in the hangingwall of the Mont Terri thrust took over the displacement (Fig. 10, step 4). It was modelled using the fault-bend-fold algorithm and a 125 m displacement. Today, this thrust is slightly folded and we envisage that the fold-nose and the internal structures developed progressively, not in discrete steps.

The initiation of the Mont Russelin culmination started with the development of the Clos du Doubs thrust, which did not propagate to the surface, but connected to the upper detachment (top of Staffelegg Formation) to form a wedge (Fig. 10, step 6). This wedge was cut by a set of two Caquerelle thrusts that formed steep slopes and propagated through to the surface (Fig. 10, steps 8 and 9). Note that in this scenario the upward bend of the beds just below the Caquerelle thrust are not caused by drag due to thrusting, but by folding due to movement over the Clos du Doubs thrust and wedge emplacement.

The Caquerelle thrusts have a NNE-trend and are interpreted to have a large component of oblique displacement. The trend of the structures and the azimuth of displacement are not within the plane of section and hence the deformation algorithms in 2D are not sufficient to model these structures, which would require a 3D forward model. The geometries of this step in section are constructed and not forward modelled. Based on current observations at the surface and in the tunnel, we interpret the structures to detach along the Triassic evaporites, but with significant deformation within the Opalinus Clay causing local thickness increase.

5.3.3 Role of inherited basement architecture

In the classic scenario, inherited basement structures are expected to play a significant role in dictating the location of both thrusts and oblique (cross) faults. Structures of both Mont Terri and Mont Russelin are thought to be triggered by relief in basement blocks, first recognised by Laubscher (1985). Fractures and faults in the overlying units may result from basement faults by either differential compaction of the (Permo-Carboniferous?) graben fills, or by possible reactivation (inversion, or strike slip) of the basement faults. These fractures and faults form weaknesses that cause nucleation of thrusts. In our current view, both Mont Terri and Mont Russelin are located just NW of interpreted basement faults, north of which compaction of the graben fill may have caused sag and a local draping tilt and/or small-scale extensional faulting of the overlying sediments (Fig. 10, step 1). This differential compaction and/or extensional fractures may explain the 180 m difference between the level of the units in the hangingwall of the Mont Terri thrust and the regional reference level (see Fig. 5).

5.3.4 Shortening estimates

The shortening (expressed as S in Fig. 10) along this section associated with the development of the Mont Terri and the Clos du Doubs thrusts is 1.725 km and 0.2 km, respectively. The development of the Caquerelle (out-of-section) thrust indicates at least another 1.0 km of shortening. The total shortening of this section amounts to 2.925 km.

5.4 Alternative scenario with duplication of sub-Opalinus Clay formations

Inspired by the recent study of Schori et al. (2015), we also propose an alternative model using multiple detachments within both the Triassic evaporites (basal detachment) and the Rietheim Member, which belongs to the top of the Staffelegg Formation (upper detachment). The presence of regional structural uplifts in the Jura, specifically in the Chasseral area of the Haute Chaîne, led Schori et al. (2015) to propose an alternative scenario to the classical view that

associates basement highs with thick-skinned tectonics (e.g. Guellec et al. 1990; Pfiffner et al. 1997), or with inherited basement normal faults causing a basement topography in horsts and grabens. They interpreted the overall structure of the Chasseral to be the result of the combination of displacements along the basal décollement in Middle Triassic evaporites and along an upper detachment at the base of the Opalinus Clay. In combination with an excess-area graphical approach and kinematic forward modelling, they argued that structural highs could have been formed during the main thin-skinned deformation, without the need for subsequent thick-skinned reactivation of pre-Triassic basement or detachment folding with thickening of anticline cores by flow of Triassic evaporites. Stratigraphic duplication by thrusting along the basal detachment that steps up to connect to a shallower detachment could explain the 180 m uplift from the regional level of the units in the Mont Terri hangingwall. Similarly, we consider here an alternative scenario involving an upper detachment within the Rietheim Member of the Staffelegg Formation (see Fig. 3). This member is composed of bituminous, predominantly thinly bedded shale and marl layers, offering a potentially good detachment layer.

5.4.1 Thrust sequence

In the duplication scenario, the thrust sequence is *overall* similar to that of the classic scenario and to the cross-cutting relationships as interpreted from the tectonic map (Fig. 4). The structures of the Mont Terri developed first, followed by the structures that formed the Mont Russelin, in an out-of-sequence fashion (Fig. 11). However, in contrast to the classic scenario, this scenario involves an initial 10.5 km duplication of the units below the Opalinus Clay formations, representing material that moved out of the section above the upper detachment, expressed as d (km) in Fig. 11. This duplication developed by displacement along the Triassic evaporites detachment that ramped up to connect to the top of the Staffelegg Formation, possibly initiated at where the Vellerat anticline now lies, bordering the southern part of the Delémont Basin (Fig. 11, step 1). After some 10.8 km of shortening (Fig. 11, step 2), two horses developed in front of this duplication (Fig. 11, step 3), followed by the development of the Mont Terri thrust (Fig. 11, step 4). Initially, the Mont Terri thrust detached along the lower Staffelegg Formation (Fig. 11, step 5), but with time the detachment stepped down to the Triassic evaporites again, through a ramp some 3 km to the SE (Fig. 11, step 6). This ramp formed the initial structure below what is now Mont Russelin. This is in contrast to the classic scenario where the initial structure is formed by a wedge and backthrust. The proto-Clos du Doubs culmination (Fig. 11, step 7) is then enhanced by the development of the two oblique thrusts related to the Caquerelle structural trend that induced additional shortening on the Mont Terri anticline, uplifting the Upper Triassic sediments to the surface (Fig. 11, step 8).

5.4.2 Folding mechanism

The dominant cause for folding in the duplication scenario is thrusting and hangingwall folding above a ramp. The corresponding deformation algorithm used in the forward modelling is fault-bend-folding. In addition, for the Mont Terri Thrust and associated hangingwall fold, a trishear mechanism is interpreted to have caused the overturned forelimb, similar to that of the classic scenario.

5.4.3 Roles of basement architecture and cross faults

Similar to the classic scenario, basement horst and grabens, and associated faults are interpreted to have initiated the development of thrust in the overlying units. Development of Caquerelle is here interpreted to be soft-linked to the basement faults, detaching in the Top Staffelegg, consistent with the interpreted weakness of this detachment. However, geometrically the Caquerelle faults could equally well have detached along the Triassic evaporites and be linked to basement faults. With the duplication of the units below the Opalinus Clay, there is no need for 180 m differential compaction or extensional fault displacement at basement level in front of the Mont Terri Thrust.

5.4.4 Shortening estimates

The shortening (expressed as S in Fig. 11) along this section, associated with the development of the Mont Terri and the proto-Clos du Doubs thrusts, is 12.9 and 0.5 km, respectively. Significantly, there is here more than ca. 2 km shortening compared to the classic scenario. Similar to the classic scenario, the ca. 800 m shortening along the Caquerelle thrust is a minimum estimate due to out-of-section displacement along this oblique structure. Displacement along the upper detachment (d) amounts to 10.8 km (Fig. 10, steps 3–4). The minimum shortening measured in this cross section amounts to 14.2 km.

6 Discussion

6.1 Mechanical viability

When a cross section is geometrically and kinematically viable, it does not mean that it is mechanically viable. Therefore, we undertook an initial mechanical analysis,

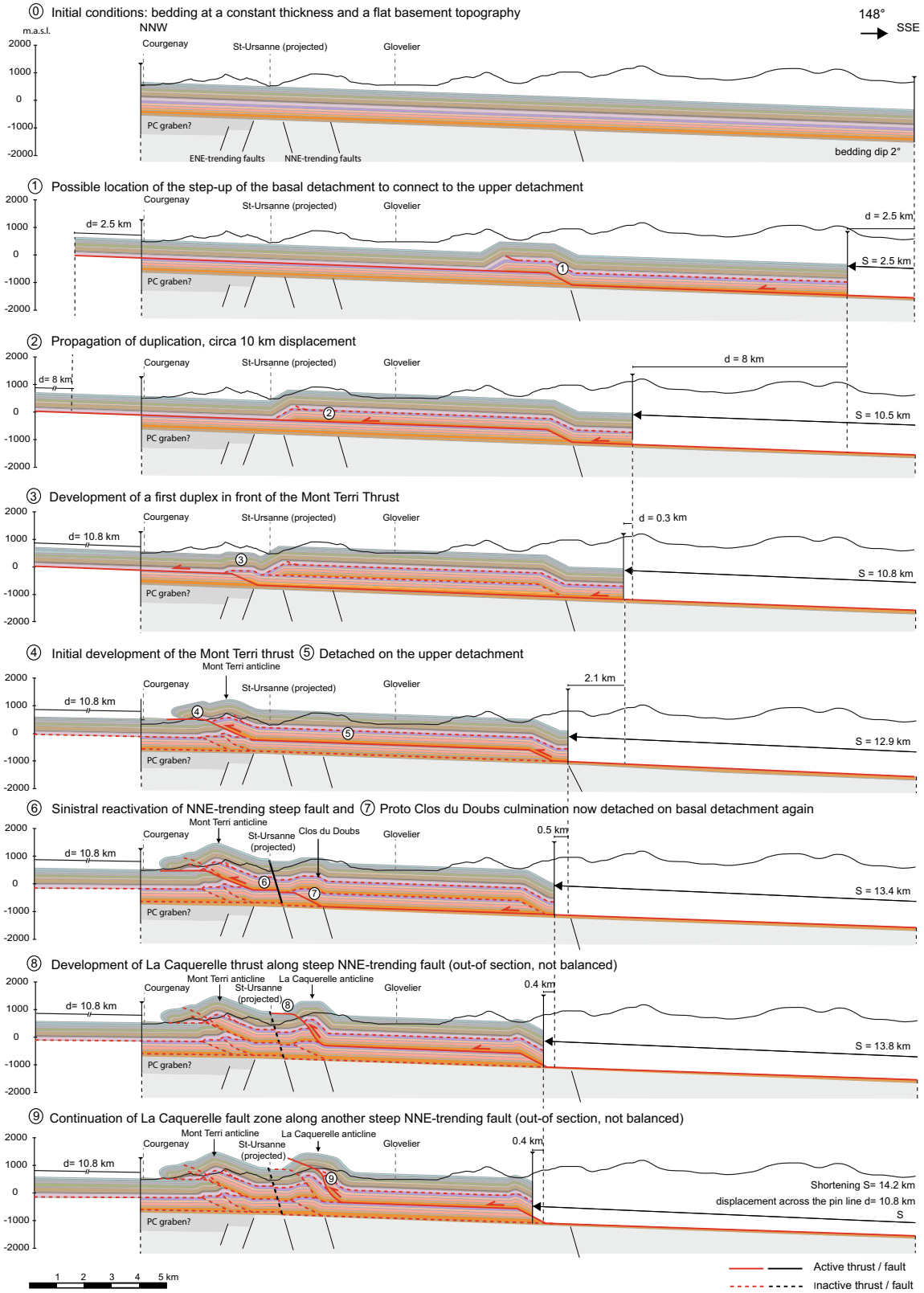

Fig. 11 Alternative forward-modelled cross section of the Mont Terri and Mont Russelin using the duplication scenario with multiple detachments: one basal detachment within the Triassic evaporites and an upper detachment at the top of the Staffelegg Formation. Section trace is shown in Figs. 2 and 4 and stratigraphic legend from Figs. 2 and 3. S and d express respectively the shortening and the displacement

based on simple prototypes, for the classical scenario presented in Fig. 10. For this we used the kinematic approach of limit analysis theory (Salençon 2002) with the OptumG2 software (OptumG2 2014; Krabbenhøft and Damilke 2003; Krabbenhøft et al. 2005; Lyamin et al. 2005; Souloumiac et al. 2009, 2010). The method consists in searching the velocity field, and therefore the location of the deformation, that requires the minimum tectonic force (Maillot and Leroy 2006). The objective is to test the mechanical viability of the thrust sequence, characterised by an out-of sequence thrusting that forms the Caquerelle anticline.

We ran a first experiment to determine the range of friction angle values on the décollement needed to initiate the Mont Terri ramp far away from the southern existing structures, i.e. Vellerat anticline (Fig. 1). In a second experiment, we assumed that some relief forms above the Mont Terri ramp and we determined the range of friction values on this ramp necessary to abandon it and initiate a new ramp southward, which would correspond to the Clos du Doubs/Caquerelle thrust.

The prototype for the first experiment corresponds to the situation at the end of the formation of the Vellerat anticline to the south (Fig. 12a). We simplified this structure giving it a 10° topographic slope and filling it with homogeneous material. North of the Vellerat structure, the sedimentary cover is modelled as flat and lying above the basement represented by homogeneous material. The topographic slope has $\alpha = 2°$ due to the presence of Cenozoic molasse (not represented on the geometrical evolution). The Triassic décollement is modelled by a horizontal plane at the base of the sedimentary cover and is disrupted by two normal faults, as in the geometrical model (Fig. 12a). We applied a compressive force along the southern wall of the prototype from the surface to the depth of the Triassic décollement. The software optimizes the value of this force by finding the geometry of failure that yields the minimum possible force. We varied the friction on the décollement Φ_d between 0° and 25°. For $\Phi_d \leq 5°$, deformation propagates beyond the northernmost normal fault, despite the disruption of the décollement level (case A in Fig. 12b, c). For $6° \leq \Phi_d \leq 7°$, the northern normal fault localizes the ramp (case B in Fig. 12b, c), as assumed by the geometrical scenario. For $8° \leq \Phi_d \leq 9°$, the southernmost normal fault localizes the ramp (case C in Fig. 12b, c). For $\Phi_d \geq 9.5°$, deformation does not propagate far enough along the décollement level to be consistent with the geometrical hypothesis presented in this paper (case D in Fig. 12b, c). In a second experiment, we choose $\Phi_d = 7°$, i.e. in the range that gives the expected result (case B Fig. 12b, c) for the first experiment. The prototype for the second experiment corresponds to the situation after ca. 2.5 km of shortening has been accommodated by sliding on the Mont Terri ramp, assuming arbitrary erosion. The mechanical test consisted in varying the friction on the part of the ramp that is in contact with the Triassic evaporites, Φ_r (purple dashed line called "Ramp part 2", Fig. 13a). The other part has a friction fixed to $\Phi_R = 18°$ (blue dashed line called "Ramp part 1", Fig. 13a). We obtained two different results. For $\Phi_r \leq 8°$, the Mont Terri ramp stays active (case B in Fig. 13c). For $\Phi_r \geq 9°$, the Mont Terri ramp is abandoned and a new ramp develops southward (case C in Fig. 13c). This last case corresponds to the hypothesis of the geometrical scenario.

These two experiments show that two main steps of the geometrical scenario are mechanically viable using our calculation procedure. The first step requires friction on the Triassic décollement that is low enough to propagate the deformation northward up to the northern normal fault, but high enough to prevent the propagation of the deformation beyond this normal fault. The results of the second experiment show that if the friction on the ramp is high enough, this ramp can be abandoned in favour of the development of a new ramp in the south. It is interesting to note that if the friction angle on the ramp is around the limit (8° or 9°), it is likely that both Mont Terri and Caquerelle structures grew simultaneously since the results suggest that the force necessary to develop the solutions B and C (Fig. 13) is almost the same. The values determined here should not be considered as absolute values, because of the many simplifications done in these models, but they have relative significance. We note, however, that the low friction values obtained here for the Triassic décollement are in accordance with those obtained by von Hagke et al. (2014) for the Triassic evaporites and shales.

Step (b) of the duplication scenario is shown in Fig. 11 (step 2). We ran an initial test to check mechanical viability and the first results show that the proposed kinematics require lower friction on the Triassic décollement than on the Staffelegg décollement, which, at first glance, is not consistent with the rheology. However, some additional factors, for instance fluid pressure, could have lowered the friction along the Staffelegg décollement. Their integration in the mechanical analysis would be an important improvement to better simulate activation of the upper detachment, which was beyond the scope of this study.

6.2 Comparison with field data and improving the kinematic forward models

In Fig. 14, we compare the modelled section for the classical scenario (Fig. 10) with the field data shown in Fig. 5. In general, the match between the data and the model is acceptable, especially for the position of the first-order thrusts and faults. The observed offset of the stratigraphic units along the Mont Terri and Mont Russelin, when present, never exceeds 100 m. At that stage, it should be

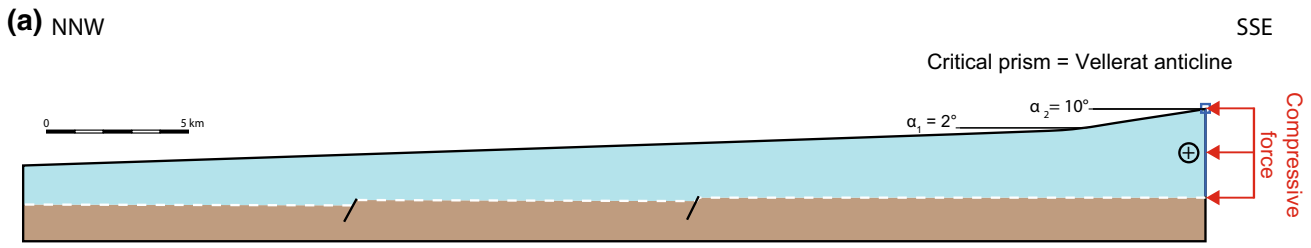

Legend	Geological units	Friction angle Φ (°)	Cohesion c (MPa)	Density ρ (kg/m³)
Sedimentary cover undifferenciated		40	5	2300
Middle Triassic detachment		*variable*	-	2300
Basement undifferenciated		45	5	2300
Extensional fault		20	-	2300

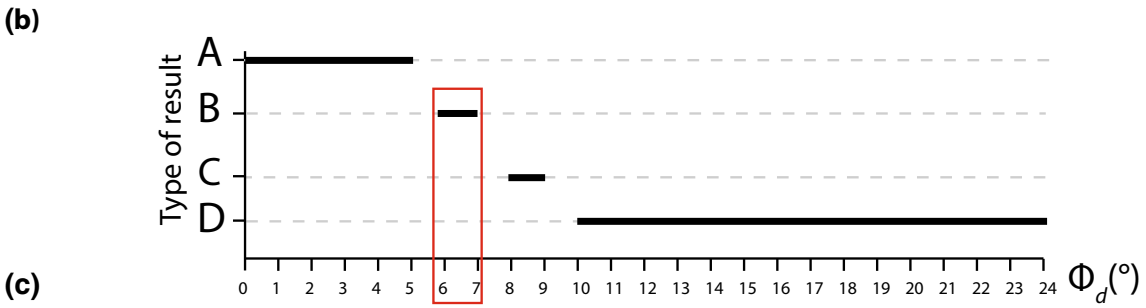

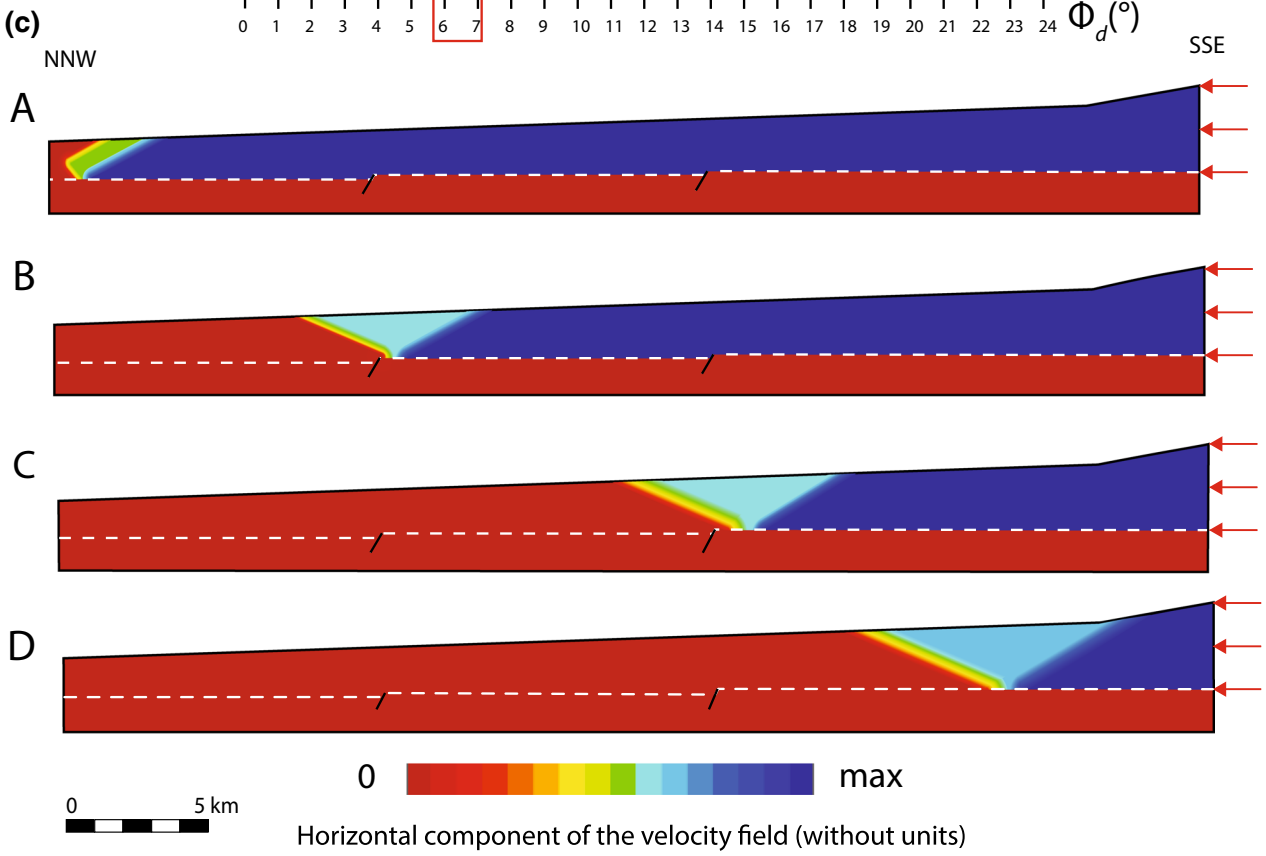

◀**Fig. 12** Results of the first geo-mechanical experiment: emplacement of the Mont Terri ramp. **a** Prototype composed of a Meso-Cenozoic sedimentary cover on top of a Triassic evaporitic décollement (*white dashed line*), lying above the basement. **b** Graph of the results obtained after applying a compressive force on the southern wall depending on the friction angle on the Triassic décollement. The *red rectangle* highlights the range of friction angles on the décollement for which the result obtained is the one expected by the geometrical scenario. **c** Illustration of the different results obtained and presented in (**b**). See text for further explanation

recalled that our model includes all geological formations individually, insuring the maximum possible detail. A grouping of certain formations together (i.e. Early-, Middle-Late Triassic, Early-, Middle-, Late Jurassic) would help to better fit the data. Another observation concerns the backlimb of the Mont Terri anticline, which is not steep enough in our modelled section. We have considered only the first-order thrusts and faults in the cross section for the purpose of this modelling study; an underestimation of the role of backthrusts could explain this discrepancy.

The use of the Trishear algorithm to model folds produces considerable thickness variations of beds that initially had a constant thickness. This is particularly clear in the forward model presented in Fig. 9. We used this algorithm to try to reproduce the present-day geometry of the overturned forelimb of the Mont Terri anticline. Field data do not support thickness thinning in the competent limestone units which are still intensively fractured. By contrast, incompetent marl units, often hidden by Quaternary sediments, show thickness changes. We suspect that the position of the present-day Folded Jura front to the north of the Mont Terri region was dictated by ENE-trending north-vergent extensional flexures (as assumed in Fig. 10, step 1) caused by the Eo-Oligocene reactivation of Permo-Carboniferous basement faults that accommodated sinistral movements in addition to the throw. Introduction of this pre-thrusting flexure in the forward model may have a positive effect by promoting development of the overturned forelimb. This would improve the geometry of the hangingwall of the Mont Terri anticline by reducing the trishear component in the modelling, thus keeping the bed thicknesses more constant as observed in the field. The use of the Trishear algorithm may not be fully appropriate in this case.

6.3 Kinematic evolution

The kinematic approach suggests an early-stage formation of the Mont Terri thrust followed by back-stepping of the deformation to develop the Caquerelle thrust further to the south. In our interpretation, possible pre-existing inherited structures may have controlled the localisation of the front of the Folded Jura. When deformation propagated to the north, it may have localised along a suspected north-dipping ENE-trending extensional flexure, perhaps caused by the Eo-Oligocene reactivation of Permo-Carboniferous faults. This gentle flexure might be a mechanical reason for the interruption of the northwards propagation of the deformation and the initiation of the Mont Terri thrust ramp that forms the present-day front of the Folded Jura. Finally, oriented at high angle from the transport direction, the oblique NNE-trending Rhenish fault beneath the Mont Russelin triggered the development of Caquerelle anticline.

In both the classical and the alternative models presented in this paper, the branch points (referring to the location at which a thrust branches off the detachment horizon) are supposed to be located above inherited basement faults. We suggest that these pre-existing faults have triggered the formation of wedges (Clairmont and Clos du Doubs) and have served as nuclei for the ramps related to the deep duplexes during a purely thin-skinned deformation. The basement topography may be either flat or offset by these inherited faults.

6.4 Open questions and recommendations for future work

The structural level of the stratigraphic sequence in the hangingwall syncline between the Mont Terri and Caquerelle anticlines is taken to indicate relative uplift of stratigraphy of ca. 180 m compared to the footwall and the presumed regional reference level to the north in the Ajoie plain. It remains questionable if this tectonic high is due to an extensional flexure above reactivated ENE-striking inherited faults during Eo-Oligocene and/or to differential compaction of the supposed Permo-Carboniferous sediments. This was the initial condition used for the construction of our classical model. Alternatively, the structural high might be explained by the duplication of a part of the sedimentary sequence (Middle Triassic-Liassic formations), by activation of an upper detachment located at the top of the Staffelegg Formation. We used this assumption to construct the alternative scenario for which the basement topography is supposed to be flat. Both scenarios propose a geometrical and viable kinematic solution.

Forward modelling of the alternative model implies that material was transported 10.5 km along the upper detachment. It is not yet clear where this shortening might have been accommodated. According to Burkhard (1990), the total shortening cumulated over the Central Jura is in the order of 25 km, based on the classical scenario with one single basal detachment. Already half of this shortening would be accommodated by our alternative model that involves only the last two anticlines of the Jura belt. The alternative model should be tentatively extended to the whole Central Jura from the Molasse Basin to the Folded Jura front to the north. As our study has shown, the basement inheritance led to a complex 3D fault and fold pattern. High-seated anticlines found everywhere in the

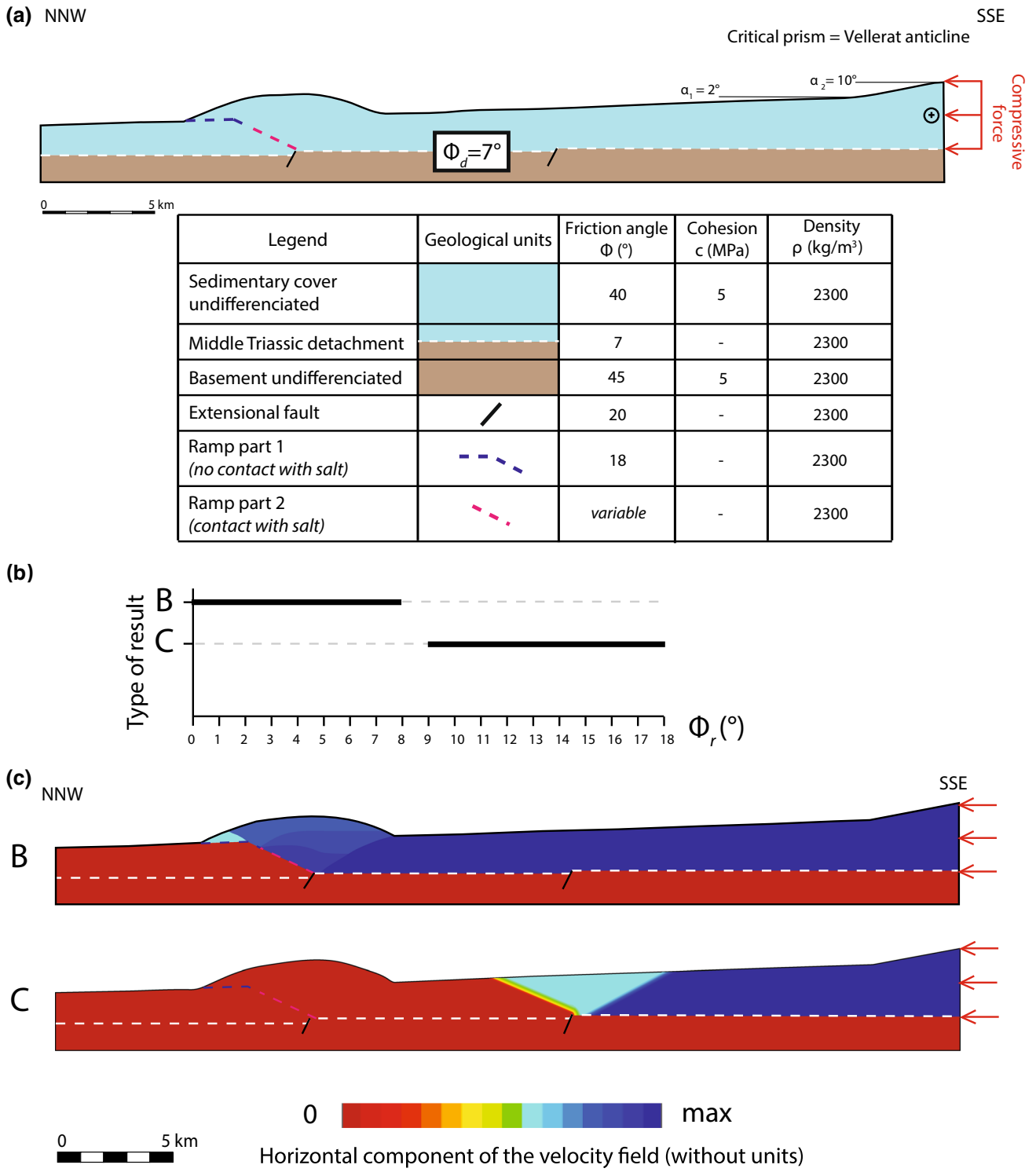

Legend	Geological units	Friction angle Φ (°)	Cohesion c (MPa)	Density ρ (kg/m³)
Sedimentary cover undifferenciated		40	5	2300
Middle Triassic detachment		7	-	2300
Basement undifferenciated		45	5	2300
Extensional fault		20	-	2300
Ramp part 1 *(no contact with salt)*		18	-	2300
Ramp part 2 *(contact with salt)*		*variable*	-	2300

Fig. 13 Results of the second geo-mechanical experiment: emplacement of the Clos-du-Doubs Caquerelle structure by abandonment of the Mont Terri ramp. **a** Same prototype as in Fig. 10 after about 2.5 km of shortening accommodated on the Mont Terri ramp. **b** Graph of the results obtained after applying a compressive force on the southern wall depending on the friction angle on the part of the ramp in contact with the Triassic evaporites. **c** Illustration of the different results obtained and presented in (**b**)

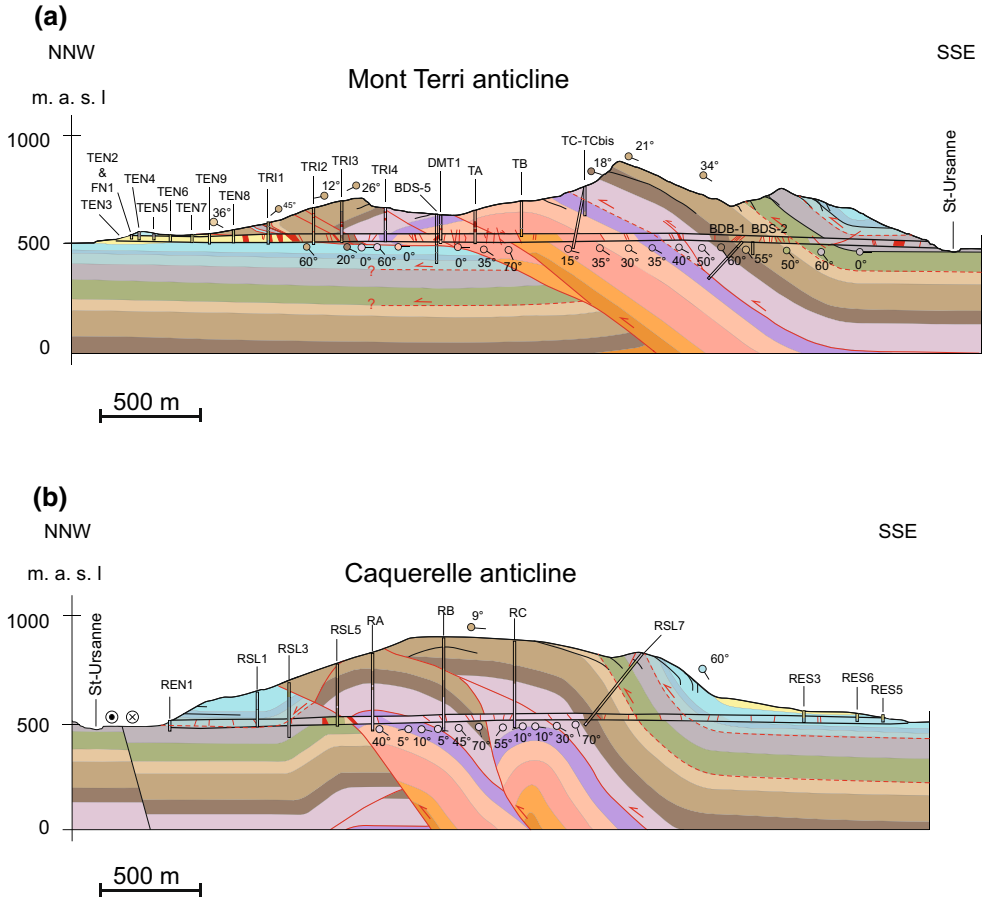

Fig. 14 Comparison of observed and forward modelled geometry, showing superposition of the tunnel, borehole and surface data (refer to Fig. 5) onto the forward modelled section shown in Fig. 10

Haute-Chaîne Folded Jura require attention and are here tentatively correlated with upper detachment levels. We suspect that any duplications are laterally controlled, segmented, and limited by NNE-trending faults or ENE-trending towards the Jura front. This may open the field for additional forward modelling. Finally, the integration of earthquake data and analysis of focal mechanisms in the forward models will help to constraint them by checking if the spatial distribution of the recent seismicity correlate with the thrusts. Both models show that subtle relationships with pre-existing basement structures might have interfered in time and in space. Both may have played a role, with lateral variation being most important.

7 Conclusions

Combining the available geological data collected in the Mont Terri and Mont Russelin tunnels, reconnaissance boreholes, cross section area balancing techniques, and kinematic forward modelling, we propose a sequential kinematic model of the region around the Mont Terri rock laboratory. Our preferred model is based on the classical interpretation along two distinct profiles involving the basal detachment within the Triassic evaporites as single décollement. This model is in good agreement with the available subsurface data. We also present an alternative model using multiple detachments: within the Triassic evaporites (basal detachment) and within the Rietheim Member belonging to the top of the Staffelegg Formation (upper detachment).

7.1 Kinematic evolution

For both scenarios, the kinematic analysis suggests an early-stage formation of the Mont Terri anticline followed by back stepping of the deformation to the south with the development of wedges (classical scenario) or deep duplexes (alternative scenario), and finally the Caquerelle thrusts which developed out-of-section.

7.2 Structural style

In the classical scenario, both anticlines (Clairmont and Clos du Doubs) located south of the Mont Terri anticline

are interpreted as wedges composed of a major foreland-facing thrust rooting in the Triassic evaporites and a backthrust rooting in the top of the Staffelegg formation, pointing towards the importance of secondary detachments. This geometry may result from the early-stage formation of the Mont Terri anticline to the north, which may have influenced the deformation style in the hinterland. We interpret the thrust sequence obtained by forward modelling to indicate the presence of at least two different sets of inherited basement faults that might have acted as nuclei for the main ramps (Mont Terri and Caquerelle thrusts) and have triggered the formation of wedges (Clairmont and Clos du Doubs). The Mont Terri anticline is interpreted to have developed above ENE-trending faults of Late Palaeozoic origin that were subsequently reactivated during the Eo-Oligocene rifting phase associated with the opening of the Rhine and Bresse graben systems. In contrast, we interpret the Caquerelle thrust to have been triggered by an E-dipping, NNE-trending fault related to the opening of the Paleogene Upper Rhine Graben. The NNE orientation of Caquerelle anticline suggests an "in situ" formation above a pre-existing structure. The anticline axis is largely oblique with respect with the NNW-shortening direction, leading to lateral displacement of material, and making it impossible to balance the cross section.

In the alternative scenario, the Mont Terri anticline and Caquerelle thrust developed above deep duplexes composed of sub-Opalinus Clay formations, the Clos du Doubs anticline being one of them. Here again, we suggest that duplex ramps might have been triggered by inherited basement faults. We note that we have supposed these inherited basement faults, they have to date not been evidenced by any field data.

7.3 Shortening estimates

The forward model for the classical scenario reveals a total shortening of 2.9 and 1.7 km for the Mont Terri anticline itself. The cross section is not totally balanced due to the lateral displacement of the Caquerelle thrust and thus the total estimated shortening represents a minimum value. The shortening found for the Mont Terri anticline lies in the range estimated to be 2.1 and 1.3 km by Freivogel and Huggenberger (2003) and Caër et al. (2015), respectively. The forward model for the alternative scenario indicates a total shortening of 14.2 km, whereby only 2.9 km are needed to form the fault-bend folds of the Mont Terri and Caquerelle. Forward modelling suggests that material was transported 10.8 km along the upper detachment. Only a limited part of this shortening could be accommodated in-section further north in the Tabular Jura where some folding is observed. It is not clear where the main part of the shortening might have been accommodated. This makes this scenario highly questionable.

7.4 Mechanical viability

We tested the mechanical viability of the thrust sequence scenario resulting from the kinematic forward modelling by applying the limit analysis mechanical approach to both the classical scenario with the basal detachment within the Middle Triassic evaporites and the alternative scenario with multiple detachments. We could validate the mechanical viability of the classic scenario. The mechanical viability of both the thrust angles and thrust sequence was demonstrated by applying the limit analysis theory. Preliminary results testing the alternative scenario show that the out-of-sequence thrust order requires lower friction along the Triassic detachment than on the Staffelegg detachment. At first glance, this is not consistent with the rheology. However, some additional factors, like fluid pressure, could have lowered the friction on the Staffelegg décollement. Their integration in the mechanical analysis would be an important improvement to better simulate the activation of the upper detachment, which was beyond the scope of this study.

Acknowledgements The authors would like to thank the Mont Terri Project Partners and especially swisstopo for their financial contribution. Both reviewers Jon Mosar and Urs Eichenberger provided useful comments and helped to improve the manuscript. Many geologists (i.e. David Jaeggi, Nicolas Badertscher, Herfried Madritsch, Andrea Lisjak) have contributed to the geological mapping of tectonic structures in the Mont Terri rock laboratory. We thank Caroline Hirsiger and Emilie Carrera for creating and improving the figures of this study, and Roy Freeman who did the English proofreading of the final version.

References

Allmendinger, R. W. (1998). Inverse and forward numerical modeling of trishear fault propagation folds. *Tectonics, 17,* 640–656.

Becker, A. (2000). The Jura Mountains: an active foreland fold-and-thrust belt? *Tectonophysics, 321,* 381–406.

Bergerat, F., & Chorowicz, J. (1981). Etude des images Landsat de la zone transformante Rhin-Saône (France). *Geologische Rundschau, 70*(1), 354–367.

Bitterli, P. (2012). Die Ifenthal-Formation im nördlichen Jura. *Swiss Bulletin for Applied Geology, 17*(2), 93–117.

Bläsi, H. R., Peters, T. J., & Mazurek, M. (1991). *Der Opalinus Clay des Mont Terri (Kanton Jura): Lithologie, Mineralogie und*

physiko-chemische Gesteinsparameter. Nagra Interner Bericht, 90-60, 44 pp. Nagra, Wettingen, Switzerland. www.nagra.ch.

Bossart, P., Bernier, F., Birkholzer, J., Bruggeman, C., Connolly, P., Dewonck, S., Fukaya, M., Herfort, M., Jensen, M., Matray, J-M., Mayor, J. C., Moeri, A., Oyama, T., Schuster, K., Shigeta, N., Vietor, T., & Wieczorek, K. (2017). Mont Terri rock laboratory, 20 years of research: introduction, site characteristics and overview of experiments. *Swiss Journal of Geosciences*, *110*. doi:10.1007/s00015-016-0236-1 (this issue).

Bossart, P., & Thury, M. (2008). *Mont Terri rock laboratory. Project, programme 1996–2007 and results*. Reports of the Swiss Geological Survey, No. 3, 445 pp. Federal Office of Topography (swisstopo), Wabern, Switzerland. www.mont-terri.ch.

Boyer, S. E., & Elliot, D. (1982). Thrust systems. *American Association of Petroleum Geologists Bulletin, 66,* 1196–1230.

Bureau Technique Norbert Geologues-Conseils SA. (1993). *Tunnel du Mont Terri Russelin—Dossier géologie après exécution*. Internal report.

Bureau Technique Jean Norbert Geologues SA, Frutiger, J.-J., Schaeren, G., & Neipp, S. (1992). *Tunnel du Mont Russelin—Notice d'accompagnement au profil géologique 1:5000 après exécution*. Internal report.

Burkhalter, R. M. (1996). Die Passwang-Alloformation (unteres Aalénien bis unteres Bajocien) im zentralen und nördlichen Jura. *Eclogae Geologicae Helvetiae, 89*(3), 875–934.

Burkhard, M. (1990). Aspects of the large scale Miocene deformation in the most external part of the Swiss Alps (Subalpine Molasse to Jura fold belt). *Eclogae Geologicae Helvetiae, 83,* 559–583.

Butler, R. W. H., Tavarnelli, E., & Grasso, M. (2006). Structural inheritance in mountain belts: An Alpine-Apennine perspective. *Journal of Structural Geology, 28,* 1893–1908.

Buxtorf, A. (1907). Zur Tektonik des Kettenjura. Berichte über die Versammlungen des Oberrheinischen. *Geologischen Vereins, 40,* 29–38.

Caër, T., Maillot, B., Souloumiac, P., Leturmy, P., Frizon de Lamotte, D., & Nussbaum, C. (2015). Mechanical validation of balanced cross sections: The case of the Mont Terri anticline at the Jura front (NW Switzerland). *Journal of Structural Geology, 75,* 32–48.

Cederboom, C. E., van der Beek, P., Schlunegger, F., Sinclair, H. D., & Oncken, O. (2011). Rapid extensive erosion of the North Alpine foreland basin at 5–4 Ma. *Basin Research, 23*(5), 528–550.

Chapple, W. M. (1978). Mechanics of thin-skinned fold-and-thrust belts. *Geological Society of America Bulletin, 89,* 1189–1198.

Comment, G., Ayer, J., & Becker, D. (2011). Deux nouveaux membres lithostratigraphiques de la Formation de Reuchenette (Kimméridgien, Ajoie, Jura Suisse)—Nouvelles données géologiques et paléontologiques acquises dans le cadre de la construction de l'autoroute A16 (Transjurane). *Swiss Bulletin for Applied Geology, 16*(1), 3–24.

Dahlen, F. A. (1990). Critical taper model of fold-and-thrust belts and accretionary wedges. *Annual Review of Earth and Planetary Sciences, 18,* 55–99.

Davis, D., Suppe, J., & Dahlen, F. A. (1983). Mechanics of fold-and-thrust belts and accretionary wedges. *Journal of Geophysical Research, 88,* 1153–1172.

Deichmann, N. (1990). *Seismizität der Nordschweiz, 1980–1988, und Auswertung der Erdbebenserien von Günsberg, Läufelfingen und Zeglingen*. Nagra Technischer Bericht, 90-46, 90 pp. Nagra, Wettingen, Switzerland. www.nagra.ch.

Erslev, E. A. (1991). Trishear fault-propagation folding. *Geology, 19,* 617–620.

Freivogel, M., & Huggenberger, P. (2003). Modellierung bilanzierter Profile im Gebiet Mont Terri-La Croix (Kanton Jura). In P. Heitzmann & J.-P. Tripet (Eds.), *Mont Terri Project-geology, paleohydrology and stress field of the Mont Terri region* (pp. 7–44). Federal Office for Water and Geology (FOWG), Geology Series, No. 5, 319 pp. www.mont-terri.ch.

Giambiagi, L. B., Alvarez, P. P., Godoy, E., & Ramos, V. A. (2003). The control of pre-existing extensional structures on the evolution of the southern sector of the Aconcagua fold and thrust belt, southern Andes. *Tectonophysics, 369,* 1–19.

Gonzalez, R., & Wetzel, A. (1996). Stratigraphy and paleogeography of the Hauptrogenstein and Klingnau Formations (middle Bajocian to late Bathonian), northern Switzerland. *Eclogae Geologicae Helvetiae, 89*(2), 695–720.

Guellec, S., Mugnier, J., Tardy, M., & Roure, F. (1990). Neogene evolution of the western Alpine foreland in the light of ECORS data and balanced cross sections. *Mémoires de la Société géologique de France, 156,* 165–184.

Gygi, R. A. (1969). Zur Stratigraphie der Oxford-Stufe (oberes Jura-System) der Nordschweiz und des süddeutschen Grenzgebietes. *Beiträge zur Geologischen Karte der Schweiz, 136,* 1–123.

Hindle, D. (2008). How hard were the Jura mountains pushed? *Swiss Journal of Geosciences, 101,* 305–310.

Homberg, C., Bergerat, F., Philippe, Y., Lacombe, O., & Angelier, J. (2002). Structural inheritance and cenozoic stress fields in the Jura fold-and-thrust belt (France). *Tectonophysics, 357,* 137–158.

Hostettler, B., Reisdorf, A. G., Jaeggi, D., Deplazes, G., Bläsi, H. R., Morard, A., Feist-Burkhardt, S., Waltschew, A., Dietze, V., & Menkveld-Gfeller, U. (2017). Litho- and biostratigraphy of the Opalinus Clay and bounding formations in the Mont Terri rock laboratory (Switzerland). *Swiss Journal of Geosciences*, *110*. doi:10.1007/s00015-016-0250-3 (this issue).

Illies, J. H. (1981). Mechanism of Graben formation. *Tectonophysics, 73,* 249–266.

Jaeggi, D., & Bossart, P. (2016). *Borehole BDS-5 near Derrière-Monterri, Courgenay, Switzerland*. Report of the Swiss Geological Survey No. 6. Federal Office of Topography (swisstopo), Wabern, Switzerland. www.mont-terri.ch. 189 pp.

Jaeggi, D., Laurich, B., Nussbaum, C., Schuster, K., & Connolly, P. (2017). Tectonic structure of the "Main Fault" in the Opalinus Clay, Mont Terri rock laboratory (Switzerland). *Swiss Journal of Geosciences*, *110*. doi:10.1007/s00015-016-0243-2 (this issue).

Jordan, P. (1992). Evidence for large-scale decoupling in the Triassic evaporites of Northern Switzerland—An overview. *Eclogae Geologicae Helvetiae, 85,* 677–693.

Krabbenhøft, K., & Damkilde, L. (2003). A general non-linear optimization algorithm for lower bound limit analysis. *International Journal for Numerical Methods in Engineering, 56,* 165–184.

Krabbenhøft, K., & Lyamin, A. V. (2014). Optum G2. *Optum Computational Engineering*. www.optumce.com.

Krabbenhøft, K., Lyamin, A. V., Hjiaj, M., & Sloan, S. W. (2005). A new discontinuous upper bound limit analysis formulation. *International Journal for Numerical Methods in Engineering, 63,* 1069–1088.

Lacombe, O., Angelier, J., Byrne, D., & Dupin, J. (1993). Eocene-Oligocene tectonics and kinematics of the Rhine-Saone continental transform zone (Eastern France). *Tectonics, 12,* 874–888.

Laubscher, H. P. (1961). Die Fernschubhypothese der Jurafaltung. *Eclogae Geologicae Helvetiae, 54,* 221–280.

Laubscher, H. P. (1963). *Erläuterungen zum Geologischen Atlasblatt "1085 St-Ursanne, 1:25'000"*. Basel: Schweizerische Geologische Kommission. Federal Office of Topography (swisstopo), Wabern, Switzerland.

Laubscher, H. P. (1963). *Geologischer Atlas der Schweiz, Atlasblatt 40, 1085 St. Ursanne—Erläuterungen.* Basel: Schweizerische Geotechnische Kommission. Federal Office of Topography (swisstopo), Wabern, Switzerland. www.mont-terri.ch.

Laubscher, H. P. (1972). Some overall aspects of Jura dynamics. *American Journal of Science, 272,* 293–304.

Laubscher, H. P. (1973). Faltenjura und Rheingraben: zwei Grossstrukturen stossen zusammen. *Jahresberichte und Mitteilungen des Oberrheinischen Geologischen Vereins, 55,* 145–158.

Laubscher, H. P. (1985). *The eastern Jura: Relations between thin-skinned and basement tectonics, local and regional*. Nagra Technischer Bericht, 85-53, 30 pp. Nagra, Wettingen, Switzerland. www.nagra.ch.

Laubscher, H. P. (1987). Die tektonische Entwicklung der Nordschweiz. *Eclogae Geologicae Helvetiae, 80,* 287–303.

Laubscher, H. P. (1992). Jura kinematics and the Molasse Basin. *Eclogae Geologicae Helvetiae, 85,* 653–675.

Laubscher, H. P. (2003). Balanced sections and the propagation of décollement: A Jura perspective. *Tectonics, 22*(6). doi:10.1029/2002TC001427.

Lyamin, A., Sloan, S., Krabbenhøft, K., & Hjiaj, M. (2005). Lower bound limit analysis with adaptive remeshing. *International Journal for Numerical Methods in Engineering, 63,* 1961–1974.

Madritsch, H., Schmid, S. M., & Fabbri, O. (2008). Interactions between thin- and thick-skinned tectonics at the northwestern front of the Jura fold-and-thrust belt (eastern France). *Tectonics*, *27*(5), 1–31.

Maillot, B., & Leroy, Y. (2006). Kink-fold onset and development based on the maximum strength theorem. *Journal of the Mechanics and Physics of Solids, 54,* 2030–2059.

Marty, D. (2008). *Sedimentology, taphonomy, and ichnology of Late Jurassic dinosaur tracks from the Jura carbonate platform (Chevenez—Combe Ronde tracksite, NW Switzerland): Insights into the tidal-flat palaeoenvironment and dinosaur diversity, locomotion, and palaeoecology*. Ph.D. dissertation, University of Fribourg, Fribourg, Switzerland, 278 pp.

Mosar, J. (1999). Present-day and future tectonic underplating in the western Swiss Alps: Reconciliation of basement/wrench-faulting and décollement folding of the Jura and Molasse basin in the Alpine foreland. *Earth and Planetary Science Letters, 173*(3), 143–155.

Nussbaum, C., Amann, F., Aubourg, C., & Bossart, P. (2011). Analysis of tectonic structures and excavation induced fractures in the Opalinus Clay, Mont Terri underground rock laboratory (Switzerland). *Swiss Journal of Geosciences, 104,* 187–210.

Pfiffner, O., Erard, P. F., & Stäuble, M. (1997). Two cross sections through the Swiss Molasse Basin (line E4–E6, W1, W7, W10). In O. A. Pfiffner, P. Lehner, P. Heitzmann, S. Müller, & A. Steck (Eds.), *Deep structure of the Swiss Alps, results of NRP 20* (pp. 64–72). Basel: Birkhäuser GmbH.

Pflug, R. (1982). *Bau und Entwicklung des Oberrheingrabens (Ertrage der Forschung)*. Darmstadt: Wissenschaftliche Buchgesellschaft.

Philippe, Y. (1995). *Rampes latérales et zones de transfert dans les chaînes plissées: Géométrie, conditions de formation et pièges structuraux associés*. Ph.D. dissertation, Université de Savoie, Chambéry, France, 272 pp.

Reisdorf, A. G., Wetzel, A., Schlatter, R., & Jordan, P. (2011). The Staffelegg formation: a new stratigraphic scheme for the Early Jurassic of northern Switzerland. *Swiss Journal of Geosciences, 104*(1), 97–146.

Rotstein, Y., Schaming, M., & Rousse, S. (2005). Tertiary tectonics of the Dannemarie Basin, upper Rhine graben, and regional implications. *Internal Journal of Earth Sciences (Geologische Rundschau), 94,* 669–679.

Salençon, J. (2002). *De l'élastodsplasticité au calcul à la rupture*. Paris: Editions Ecole Polytechnique.

Schaeren, G., & Norbert, J. (1989). Tunnels du Mont Terri et du Mont Russelin —La traversée des « roches à risques » : marnes et marnes à anhydrite. *Juradurchquerungen—aktuelle Tunnelprojekte im Jura. Mitteilungen der Schweizerischen Gesellschaft für Boden- und Felsmechanik, 119,* 19–24.

Schori, M., Mosar, J., & Schreurs, G. (2015). Multiple detachments during thin-skinned deformation of the Swiss central Jura: a kinematic model across the Chasseral. *Swiss Journal of Geosciences, 108,* 327–343.

Schumacher, M. E. (2002). Upper Rhine Graben: Role of preexisting structures during rift evolution. *Tectonics*, *21*, 1006–1022. doi:10.1029/2001TC900022.

Smit, J. H. W., Brun, J. P., & Sokoutis, D. (2003). Deformation of brittle-ductile thrust wedges in experiments and nature. *Journal of Geophysical Research, 108*(B10), ETG9-1.

Sommaruga, A., & Burkhard, M. (1997). Seismic sections through the Alpine foreland—Jura Mountains. In O. A. Pfiffner, P. Lehner, P. Heitzmann, S. Müller, & A. Steck (Eds.), *Results of NRP 20—Deep structure of the Swiss Alps* (pp. 45–53). Basel: Birkhäuser GmbH.

Souloumiac, P., Krabbenhøft, K., Leroy, Y., & Maillot, B. (2010). Failure in accretionary wedges with the maximum strength theorem: Numerical algorithm and 2D validation. *Computational Geosciences, 14*(4), 793–811.

Souloumiac, P., Leroy, Y.-M., Krabbenhøft, K., & Maillot, B. (2009). Predicting stress in fault-bend fold by optimization. *Journal of Geophysical Research*, *114*.

Suppe, J. (1983). Geometry and kinematics of fault-bend folding. *American Journal of Science, 283,* 684–721.

Suppe, J., Connors, C. D., & Zhang, Y. (2004). Shear fault-bend folding. In K. R. McClay (Ed.), *Thrust tectonics and hydrocarbon systems: AAPG Memoir 82* (pp. 303–323). Tusla: American Association of Petroleum Geologists.

Suppe, J., & Medwedeff, D. A. (1990). Geometry and kinematics of fault-propagation folding. *Eclogae Geologicae Helvetiae, 83,* 409–459.

Suter, M. (1978). Geologische Interpretation eines reflexionsseismischen W-E-Profils durch das Delsberger Becken (Faltenjura). *Eclogae Geologicae Helvetiae, 71,* 267–275.

Swisstopo. (2011). *Digital elevation model swissALTI3D*. Federal Office of Topography (swisstopo), Wabern, Switzerland. www.swisstopo.ch.

Swisstopo. (2012). *GeoCover-geological vector data*. Federal Office of Topography (swisstopo), Wabern, Switzerland. www.map.geo.admin.ch.

Ustaszewsi, K., Schuhmacher, M. E., & Schmid, S. (2005). Simultaneous normal faulting and extensional flexuring during rifting: An example from the southernmost Upper Rhine Graben. *International Journal of Earth Sciences, 94,* 680–696.

Ustaszewski, K., & Schmid, S. M. (2006). Control of pre-existing faults on geometry and kinematics in the northernmost part of the Jura fold-and-thrust belt. *Tectonics*, *25*, TC5003. doi:10.1029/2005TC001915.

Ustaszewski, K., & Schmid, S. (2007). Latest Pliocene to recent thick-skinned tectonics at the Upper Rhine Graben—Jura Mountains junction. *Swiss Journal of Geosciences, 100,* 293–312.

von Hagke, C., Oncken, O., & Evseev, S. (2014). Critical taper analysis reveals lithological control of variations in detachment strength: An analysis of the Alpine basal detachment (Swiss Alps). *Geochemistry Geophysics Geosystems*, *15*(1), 176–191.

Wetzel, A., & Allia, V. (2003). Der Opalinuston in der Nordschweiz: lithologie und Ablagerungsgeschichte. *Eclogae Geologicae Helvetiae, 96,* 451–469.

Ziegler, P. A. (1992). European Cenozoic rift system. *Tectonophysics, 208,* 91–111.